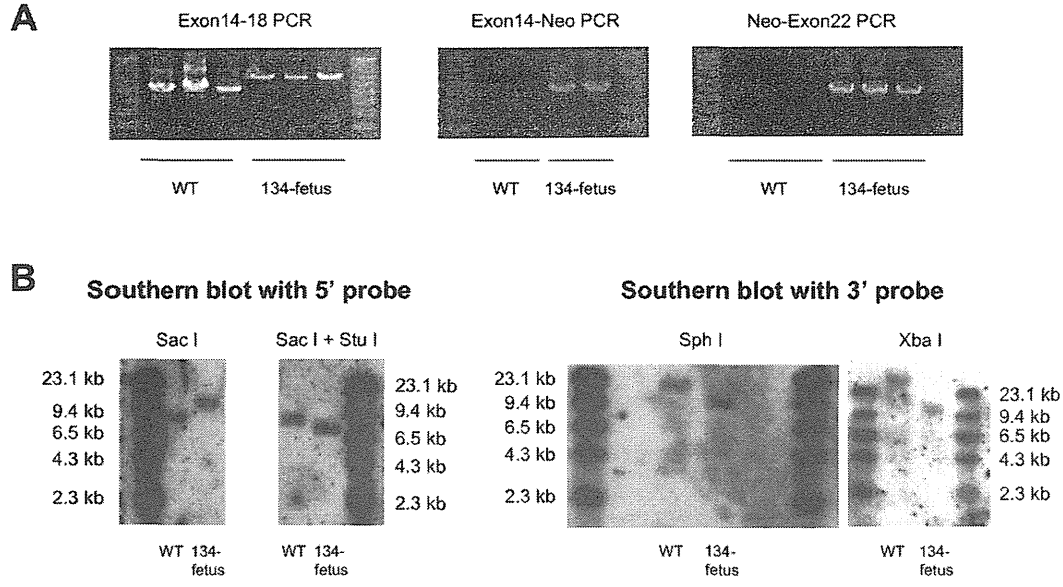

Figure 2. *F8* targeting and genetic analysis of the colony 134-derived fetus. PCR analysis of genomic DNA of 134-fetus was shown. (**A**) Two or three independent PCR reactions were carried out for detection of recombination in *F8* of 134-fetus. (**B**) Southern blotting with a 5′ exon 14 probe (on *Sac* I− or *Sac* I + *Stu* I-digested DNA) and with a 3′ exon 22 probe (on *Sph* I− or *Xba* I-digested DNA) showed correct targeting of the *F8* in 134-fetus.
doi:10.1371/journal.pone.0049450.g002

Two of the piglets (#1 and #2) found dead the next day (day 2) after delivery. The cause of death of these two piglets was not certain. Early deaths of cloned piglets after birth are not uncommon as described [24,25]. Accidental bleeding might affect the condition of piglet #1 since large hematomas were observed in piglet #1 (Figure 4). Massive traumatic intramuscular bleeding was thought to affect the death of piglet #3 on day 3 because the general condition of piglet #3 became severe immediately after the bleeding took place and piglet #3 died. Piglet #4 was born with bleeding in the left forelimb, thus, human FVIII concentrate (150 U/kg) was injected intravenously on day 2 after delivery, which cured the bleeding in the limb (Figure 4). However, because this piglet still showed a bleeding in the limbs and the tongue, which was cured with human FVIII infusion, it was given a prophylactic infusion of human FVIII (150 U/kg) twice a week, which was effective in reducing the bleeding frequency. The human FVIII activity at 12.1% (average of two points; day 10 and day 23 after birth) was detected in the piglet #4 plasma obtained two days after the injection. However, spontaneous bleeding still occurred in piglet #4, in particular repeated bleeding in the left forelimb, causing limping (Figure 4 and video S1). Piglet #4 died due to gastric bleeding from a gastric ulcer on day 38 after birth. Inhibitor (856 BU/mL) against human FVIII was detected in the plasma obtained on the day when piglet #4 died. The development of inhibitor might explain why human FVIII injected two days before was not effective to reduce bleeding from the gastric ulcer.

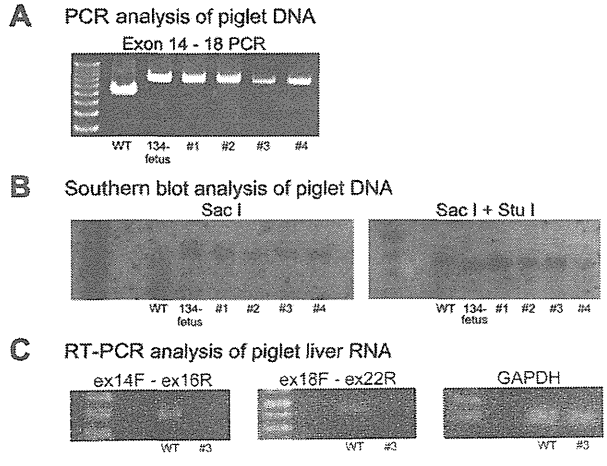

Figure 3. Analysis of the *F8* in cloned piglets. (**A**) PCR analysis of genomic DNA of piglet DNA was shown. Genomic DNA of wild-type, 134-fetus, piglet #1, piglet #2, piglet #3, and piglet #4 was subjected to PCR analysis with primers Exon 14 sF and Exon 18 sR as in Figure 1. The 8.3 kb exon 14–18 band was amplified from the 134-fetus DNA and the cloned piglet DNA. (**B**) Southern blotting with a 5′ exon 14 probe (on *Sac* I− or *Sac* I + *Stu* I-digested DNA) showed the same mobility shifts of the bands as those in Figure 2**B** and confirmed the insertion of the Neo resistant gene in *F8* of the cloned piglets. (**C**) RT-PCR analysis of piglet liver RNA was shown. Two independent PCRs (exons 14–16 and exons 18–22) revealed the absence of FVIII mRNA from the liver of cloned piglet #3. Control GAPDH mRNA was detected in the liver RNA of piglet #3 as in the wild type (WT).
doi:10.1371/journal.pone.0049450.g003

Discussion

Advances in cloning technology have allowed us to generate genetically modified animals [22,26,27]. Among these, a few gene-targeted pigs have been reported, such as cystic fibrosis pigs [28] and heterozygous fumarylacetoacetate hydrolase deficient pigs [29]as a disease model, and α1, 3-galactosyltransferase gene-knockout (KO) pigs [30] for organ transplantation [30,31]. Considering the limitations in studying human disease in murine models, gene-targeted pigs are thought to be preferred for studying

Table 1. Coagulation factor activity of piglets #3 and #4.

Coagulation factor	Wild type (n = 4)	Piglet #3	Piglet #4
Fibrinogen (μmol/L)	2.67±1.39	1.56	ND
Factor II (%)	75.7±3.9	53	47
Factor V (%)	>200	118	168
Factor VII (%)	68.5±3.4	19	19
Factor VIII (%)	>200	1>	1>
Factor IX (%)	>200	96	69
Factor X (%)	134±7.0	72	64
	Wild type (n = 4)	**Piglet #3**	**Piglet #4**
von Willebrand Factor (%)	174.7±25.9	124	251
Albumin (g/dL)	2.8±0.08	1.0	1.9
Cholinesterase (IU/L)	3.75±1.50	15	3

The coagulation factor levels of piglet #3 and #4 are shown with the control coagulation factor levels of wild-type piglets. Each coagulation factor activity was calculated from the standard curve generated with normal human plasma and expressed as the percentage of the respective coagulation factor activity in normal human plasma.
ND: not determined.
doi:10.1371/journal.pone.0049450.t001

human diseases and for translational research. We explore the possibility of *F8* KO pigs (hemophilia A pigs) for studying the next generation therapy for hemophilia A in the current study. The genotype of cloned pigs showed the proper recombination in the *F8* of the pigs and the blood coagulation factor levels of cloned pigs confirmed severe FVIII deficiency. The precise mechanism of moderately decreased other coagulation factor levels in piglets #3 and #4 was not elucidated yet, these changes may not be specific to the coagulation factors since the level of albumin was decreased but the cholinesterase level was not decreased (both albumin and cholinesterase are synthesized in the liver). One possible mechanism of the changes could be the epigenetic effect genome DNA methylation and histone acetylation, which alter gene expression in cloned pigs [24,32,33,34]. Hemophilia A pigs generated by the nuclear transfer technology did show a severe bleeding phenotype that is in contrast to *F8* KO mice that rarely exhibit spontaneous bleeding into the muscles and joints under standard breed conditions [9]. Therefore, hemophilia A pig can be used to evaluate an efficacy of novel therapy such as gene therapy for hemophilia A in a standard breed condition. Moreover, prophylactic infusion of human FVIII was effective in reducing bleeding in *F8* KO piglet #4 thought its therapeutic effect was not perfect. This suggests that the *F8* KO pig is a subhuman animal model of severe hemophilia A for the study of upcoming therapeutic factors, such novel FVIII variants. Piglet #4 died because of bleeding from a gastric ulcer. Since inhibitor against human FVIII was detected in the plasma sample obtained on the day when piglet #4 died, the therapeutic effect of human FVIII no longer existed at the time, resulting in severe bleeding from the gastric ulcer. It is possible that *F8* KO pigs might develop antibodies against porcine FVIII as against human FVIII. The possibility of the use of *F8* KO pigs as a model for studying immune tolerance induction therapy for FVIII inhibitor remains to be studied.

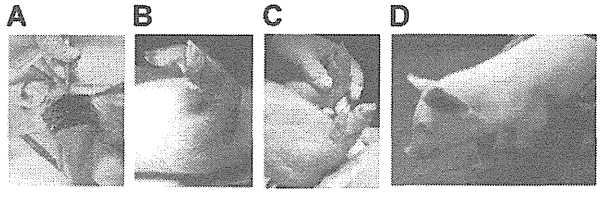

Figure 4. The bleeding phenotype of cloned *F8* KO piglets. (**A**) A part of macroscopic picture of cloned piglet #1, which died by day 2 after birth is shown. Ecchymosis was seen in the cheek, the forelimb, and the hind limb (not shown). Pathological examination revealed hematomas in these areas of piglet #1. (**B**) Forelimb of cloned piglet #4 on day 1 after delivery was shown. Ecchymosis had been seen in the left forelimb of cloned piglet #4 since delivery. (**C**) On day 5 after administration of human FVIII (150 U/kg), the bleeding in the left forelimb was not observed. Macroscopic picture of cloned piglet #4 on day 28 after birth showed that the left forelimb was swollen because of the repeated bleeding (**D**), causing the piglet to limp (also see video 1).
doi:10.1371/journal.pone.0049450.g004

Methods

Construction of the F8 targeting vector

Porcine genomic DNA was isolated from porcine embryonic fibroblasts (LW; Landrace – Large White, ED65). The *F8* targeting vector was constructed by inserting two genomic DNA fragments into the plasmid vector pHSV-TK/PGK-Neo. The *F8* targeting vector was designed by referring to the *F8* exon 16 gene-targeting vector used to generate hemophilia A mice [9]. *F8* DNA fragments from exons 14–22 were isolated by PCR using primers (Table S1) based on the *Sus scrofa* coagulation factor VIII mRNA sequence (accession number: NM_214167) and sequenced. The two homologous arms of the gene-targeting vector were generated by reference to this sequence. The 5′ DNA fragment spanning intron 15 to exon 21 of *F8* was PCR-amplified, digested with *Xho* I to generate an 11-nucleotide deletion of exon 16, and inserted into pHSV-TK/PGK-Neo. The 3′ DNA fragment was PCR-amplified from exon 16 to intron 21, and cloned into pHSV-TK/PGK-Neo containing the 5′ *F8* DNA fragment. The herpes simplex virus thymidine kinase gene was located in the opposite orientation on the 5′ end of the 5′ arm. The targeting vector was linearized with *Not* I before transfection.

Isolation of porcine embryonic fibroblasts and isolation of F8-targeted cells

Porcine embryonic fibroblasts (PEF) were isolated from a male fetus of the LW strain as described [22]. PEFs (1×10^7 cells) were transfected with the *F8* targeting vector by electroporation (Gene Pulser II; Bio-Rad, Hercules, CA) at 278 V and 950 μF. After transfection, cells were cultured in Dulbecco's modified Eagle's medium with low-glucose (Invitrogen, Carlsbad, CA) containing 10% fetal bovine serum. After 48 h incubation, cells were selected with 800 μg/ml G418 (Nacalai Tesque, Inc., Kyoto, Japan) and 2 μM gancyclovir (Tanabe-Mitsubishi Pharma, Tokyo, Japan). On the eighth day following selection, G418-resistant colonies had grown. Cells from these colonies were grown in 24-well plates (Corning) in medium containing 4 ng/ml bFGF, and expanded for genomic DNA extraction and storage. DNA isolated from three wells of each colony was analyzed by three independent PCR reactions for recombination in the porcine *F8* (Table S1).

Southern blotting

Southern blotting for the *F8* recombination was performed by the standard procedure. Digoxigenin (DIG)-labeled 5′ and 3′ probes were generated by PCR (497 bp from exon 14 and 469 bp from exon 22, respectively) (Table S1). Signals were visualized using a DIG detection module (anti-DIG-alkaline phosphatase and a CSPD) (Roche Diagnostics GmbH., Mannheim, Germany).

RT-PCR of porcine FVIII mRNA

Total RNA was isolated from piglet liver using an RNeasy Mini kit (Invitrogen), converted to cDNA and PCR amplified using the SuperScript One-Step RT-PCR System (Invitrogen) with primer pairs specific for FVIII mRNA (Table S1) [35,36].

Nuclear transfer and transplantation of manipulated embryos to recipients

Production of clone piglets by nuclear transfer was performed as described previously [22,23]. In brief, metaphase II oocytes were enucleated by gentle aspiration of the first polar body and adjacent cytoplasm using a beveled pipette (25 to 30 μm) in PZM3 medium containing 5.0 μg/ml cytochalasin B. Enucleated oocytes were washed in PZM3 medium lacking cytochalasin B and nuclei of the *F8*-targeted cells introduced by direct intracytoplasmic injection using a piezo-actuated micromanipulator (Prime Tech., Tsuchiura, Japan). Oocytes were then stimulated with a direct current pulse of 1.5 kV/cm for 100 μS using a somatic hybridizer (SSH-10, Shimadzu, Kyoto, Japan) and transferred to PZM3 supplemented with cytochalasin B to prevent extrusion of a pseudo-second polar body. The nuclear transferred oocytes were then cultured in PZM3 medium in an atmosphere of 5% CO_2, 5% O_2 and 90% air at 38.5°C for 2 days until reaching the two-to-eight-cell stage. Cleaved embryos were transferred to the oviducts (200 embryos per recipient) of an anesthetized pseudopregnant surrogate mother (matured LWD; a Landrace×Large White× Duroc triple cross). Following embryo transfer, mother pigs were observed daily to confirm pregnancy by checking estrus. Farrowing was synchronized by injection of the prostaglandin F2α analog, (l)-cloprostenol (Planate, Osaka, Japan) on day 113–116 of gestation.

Coagulation factor activity measurement

Activities of porcine coagulation factors were measured at a clinical laboratory (SRL, Tokyo, Japan) by the standard clotting time method with respective coagulation factor-deficient human plasma. Normal human plasma was used as the standard for each test. The coagulation factor activity in piglet plasma was expressed as the percentage of the coagulation factor activity in normal pooled plasma, except for fibrinogen. The fibrinogen concentration was determined by the thrombin time method. von Willebrand factor levels in pig plasma were measured with an enzyme immunoassay with latex particle conjugated antibody (performed at SRL, Tokyo, Japan) since the von Willebrand factor activity (Ristocetin cofactor activity) in pig plasma was unable to be measured with human platelets. The von Willebrand factor antigen levels in pig plasma were expressed as percentages of the normal human plasma. An inhibitor assay for human FVIII was performed as described [36].

Blood chemistry analysis

The levels of albumin and choline esterase of piglet blood were measured at the Nagahama Life-science Laboratory of Oriental East Co. Ltd (Hagahama, Shiga-ken, Japan). Choline esterase activities of blood samples were measured with p-hydroxy benzoyl choline iodide as the substrate [37].

Animal experiments

All the animal experiments and surgical procedures were carried out in accordance with guidelines approved by the Institutional Animal Care and Concern Committees of Jichi Medical University and the National Institute of Agrobiological Sciences. Protocols for the use of animals in this study were approved by the review boards of Animal Care Committees of Jichi Medical University and the National Institute of Agrobiological Sciences. Wild type pigs used in this study were bred under a standard condition according to the institutional guideline of Animal Care Committee of National Institute of Agrobiological Sciences. After delivery, cloned F8KO pigs were separated from mother pigs and each cloned F8KO pig was bred by artificial suckling in a cage with protection of soft buffers to avoid traumas. All the experimental procedures including injection of FVIII were carried out under inhalation anesthesia with isoflurane and monitoring of body temperature. The endpoint of this study was to generate F8KO pigs and analyze the genotype and the phenotype of the F8KO pig precisely to investigate whether the F8KO pig can be a subhuman model of severe hemophilia A.

Supporting Information

Table S1 Sequences of primers used in this study.
(DOC)

Video S1 Piglet #4 (day 28 after birth) to limp in the left forelimb.
(MOV)

Author Contributions

Wrote the paper: JM. Senior investigator and supervised this study: YS. Acted as a senior investigator, planned, generated constructs for F8 gene targeting, and conducted the study: JM. Postdoctoral fellow, conducted most of the F8 targeting work and injected human FVIII into a cloned piglet: YK. Performed nuclear transfer of targeted cells to oocytes and transplantation of the oocytes, and managed care of cloned pigs: AO MI. Injected human FVIII into a cloned piglet on day 1 after birth: SM. Cared for cloned piglets and did pathological examination of cloned piglets: DF SS MS SS MH SY. Performed cell culture experiments: AI AY AS TO.

References

1. Mannucci PM, Tuddenham EG (2001) The hemophilias–from royal genes to gene therapy. N Engl J Med 344: 1773–1779.
2. Manco-Johnson MJ, Abshire TC, Shapiro AD, Riske B, Hacker MR, et al. (2007) Prophylaxis versus episodic treatment to prevent joint disease in boys with severe hemophilia. N Engl J Med 357: 535–544.
3. Hasbrouck NC, High KA (2008) AAV-mediated gene transfer for the treatment of hemophilia B: problems and prospects. Gene Ther 15: 870–875.
4. VandenDriessche T, Collen D, Chuah MK (2003) Gene therapy for the hemophilias. J Thromb Haemost 1: 1550–1558.
5. Manno CS, Pierce GF, Arruda VR, Glader B, Ragni M, et al. (2006) Successful transduction of liver in hemophilia by AAV-Factor IX and limitations imposed by the host immune response. Nat Med 12: 342–347.
6. Nathwani AC, Tuddenham EG, Rangarajan S, Rosales C, McIntosh J, et al. (2011) Adenovirus-associated virus vector-mediated gene transfer in hemophilia B. N Engl J Med 365: 2357–2365.
7. Roth DA, Tawa NE Jr, O'Brien JM, Treco DA, Selden RF (2001) Nonviral transfer of the gene encoding coagulation factor VIII in patients with severe hemophilia A. N Engl J Med 344: 1735–1742.
8. Powell JS, Ragni MV, White GC 2nd, Lusher JM, Hillman-Wiseman C, et al. (2003) Phase 1 trial of FVIII gene transfer for severe hemophilia A using a retroviral construct administered by peripheral intravenous infusion. Blood 102: 2038–2045.
9. Bi L, Lawler AM, Antonarakis SE, High KA, Gearhart JD, et al. (1995) Targeted disruption of the mouse factor VIII gene produces a model of haemophilia A. Nat Genet 10: 119–121.
10. Brown BD, Shi CX, Powell S, Hurlbut D, Graham FL, et al. (2004) Helper-dependent adenoviral vectors mediate therapeutic factor VIII expression for several months with minimal accompanying toxicity in a canine model of severe hemophilia A. Blood 103: 804–810.
11. Finn JD, Ozelo MC, Sabatino DE, Franck HW, Merricks EP, et al. (2010) Eradication of neutralizing antibodies to factor VIII in canine hemophilia A after liver gene therapy. Blood 116: 5842–5848.
12. Sabatino DE, Freguia CF, Toso R, Santos A, Merricks EP, et al. (2009) Recombinant canine B-domain-deleted FVIII exhibits high specific activity and is safe in the canine hemophilia A model. Blood 114: 4562–4565.
13. Porada CD, Sanada C, Long CR, Wood JA, Desai J, et al. (2010) Clinical and molecular characterization of a re-established line of sheep exhibiting hemophilia A. J Thromb Haemost 8: 276–285.
14. Lunney JK (2007) Advances in swine biomedical model genomics. Int J Biol Sci 3: 179–184.
15. Bendixen E, Danielsen M, Larsen K, Bendixen C (2010) Advances in porcine genomics and proteomics–a toolbox for developing the pig as a model organism for molecular biomedical research. Brief Funct Genomics 9: 208–219.
16. Massicotte P, Mitchell L, Andrew M (1986) A comparative study of coagulation systems in newborn animals. Pediatr Res 20: 961–965.
17. Reverdiau-Moalic P, Watier H, Vallee I, Lebranchu Y, Bardos P, et al. (1996) Comparative study of porcine and human blood coagulation systems: possible relevance in xenotransplantation. Transplant Proc 28: 643–644.
18. Chen Y, Qiao J, Tan W, Lu Y, Qin S, et al. (2009) Characterization of porcine factor VII, X and comparison with human factor VII, X. Blood Cells Mol Dis 43: 111–118.
19. Morrison AE, Ludlam CA (1991) The use of porcine factor VIII in the treatment of patients with acquired hemophilia: the United Kingdom experience. Am J Med 91: 23S–26S.
20. Toschi V (2010) OBI-1, porcine recombinant Factor VIII for the potential treatment of patients with congenital hemophilia A and alloantibodies against human Factor VIII. Curr Opin Mol Ther 12: 617–625.
21. Barrow RT, Lollar P (2006) Neutralization of antifactor VIII inhibitors by recombinant porcine factor VIII. J Thromb Haemost 4: 2223–2229.
22. Onishi A, Iwamoto M, Akita T, Mikawa S, Takeda K, et al. (2000) Pig cloning by microinjection of fetal fibroblast nuclei. Science 289: 1188–1190.
23. Suzuki S, Iwamoto M, Saito Y, Fuchimoto D, Sembon S, et al. (2012) Il2rg gene-targeted severe combined immunodeficiency pigs. Cell Stem Cell 10: 753–758.
24. Cho SK, Kim JH, Park JY, Choi YJ, Bang JI, et al. (2007) Serial cloning of pigs by somatic cell nuclear transfer: restoration of phenotypic normality during serial cloning. Dev Dyn 236: 3369–3382.
25. Umeyama K, Watanabe M, Saito H, Kurome M, Tohi S, et al. (2009) Dominant-negative mutant hepatocyte nuclear factor 1alpha induces diabetes in transgenic-cloned pigs. Transgenic Res 18: 697–706.
26. Chesne P, Adenot PG, Viglietta C, Baratte M, Boulanger L, et al. (2002) Cloned rabbits produced by nuclear transfer from adult somatic cells. Nat Biotechnol 20: 366–369.
27. Shin T, Kraemer D, Pryor J, Liu L, Rugila J, et al. (2002) A cat cloned by nuclear transplantation. Nature 415: 859.
28. Rogers CS, Stoltz DA, Meyerholz DK, Ostedgaard LS, Rokhlina T, et al. (2008) Disruption of the CFTR gene produces a model of cystic fibrosis in newborn pigs. Science 321: 1837–1841.
29. Hickey RD, Lillegard JB, Fisher JE, McKenzie TJ, Hofherr SE, et al. (2011) Efficient production of Fah-null heterozygote pigs by chimeric adeno-associated virus-mediated gene knockout and somatic cell nuclear transfer. Hepatology.
30. Lai L, Kolber-Simonds D, Park KW, Cheong HT, Greenstein JL, et al. (2002) Production of alpha-1,3-galactosyltransferase knockout pigs by nuclear transfer cloning. Science 295: 1089–1092.
31. Yamada K, Yazawa K, Shimizu A, Iwanaga T, Hisashi Y, et al. (2005) Marked prolongation of porcine renal xenograft survival in baboons through the use of alpha1,3-galactosyltransferase gene-knockout donors and the cotransplantation of vascularized thymic tissue. Nat Med 11: 32–34.
32. Tian XC, Park J, Bruno R, French R, Jiang L, et al. (2009) Altered gene expression in cloned piglets. Reprod Fertil Dev 21: 60–66.
33. Shen CJ, Cheng WT, Wu SC, Chen HL, Tsai TC, et al. (2012) Differential differences in methylation status of putative imprinted genes among cloned swine genomes. PLoS One 7: e32812.
34. Kim YJ, Ahn KS, Kim M, Shim H (2011) Comparison of potency between histone deacetylase inhibitors trichostatin A and valproic acid on enhancing in vitro development of porcine somatic cell nuclear transfer embryos. In Vitro Cell Dev Biol Anim 47: 283–289.
35. Ishiwata A, Mimuro J, Kashiwakura Y, Niimura M, Takano K, et al. (2006) Phenotype correction of hemophilia A mice with adeno-associated virus vectors carrying the B domain-deleted canine factor VIII gene. Thromb Res 118: 627–635.
36. Ishiwata A, Mimuro J, Mizukami H, Kashiwakura Y, Takano K, et al. (2009) Liver-restricted expression of the canine factor VIII gene facilitates prevention of inhibitor formation in factor VIII-deficient mice. J Gene Med 11: 1020–1029.
37. Tanaka H, Igarashi T, Lefor AT, Kobayashi E (2009) The effects of fasting and general anesthesia on serum chemistries in KCG miniature pigs. J Am Assoc Lab Anim Sci 48: 33–38.

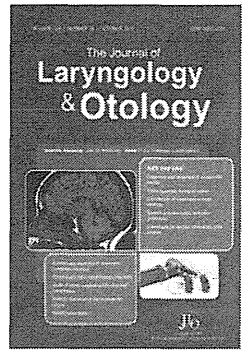

Morphological assessment of the luminal surface of olfactory epithelium in mice deficient in tissue plasminogen activator following bulbectomy

N Makino, S Ookawara, S Madoiwa, Y Ohta, T Ishikawa, K Katoh, S Takigami, T Kanazawa, O Matsuo, M Ichikawa, J Mimuro, Y Sakata and K Ichimura

The Journal of Laryngology & Otology / *FirstView* Article / October 2012, pp 1 - 7
DOI: 10.1017/S002221511200206X, Published online:

The Journal of Laryngology & Otology, 1 of 7.

doi:10.1017/S002221511200206X

MAIN ARTICLE

Morphological assessment of the luminal surface of olfactory epithelium in mice deficient in tissue plasminogen activator following bulbectomy

N MAKINO[1], S OOKAWARA[2], S MADOIWA[3], Y OHTA[1], T ISHIKAWA[1], K KATOH[2], S TAKIGAMI[4], T KANAZAWA[1], O MATSUO[5], M ICHIKAWA[6], J MIMURO[3], Y SAKATA[3], K ICHIMURA[1]

Departments of [1]Otolaryngology–Head and Neck Surgery and [2]Anatomy, and [3]Division of Cell and Molecular Medicine, Center for Molecular Medicine, Jichi Medical University School of Medicine, Shimotsuke, Tochigi, [4]Laboratory of Anatomy and Cellular Biology, Department of Medical Technology, Faculty of Health Sciences, Kyorin University, Hatioji, Tokyo, [5]Department of Physiology II, Kinki University School of Medicine, Osakasayama City, and [6]Laboratory of Anatomy and Cell Biology, Department of Neuroscience Basic Technology, Tokyo Metropolitan Institute for Neuroscience, Fuchu, Tokyo, Japan

Abstract

Objective: This study aimed to investigate the function of tissue plasminogen activator in the olfactory epithelium of mice following neural injury.

Method: Transmission electron microscopy was used to study the changes in the morphology of the olfactory epithelium 1–7 days after surgical ablation of the olfactory bulb (bulbectomy).

Results: Prior to bulbectomy, a uniformly fine material was observed within some regions of the olfactory epithelium of mice deficient in tissue plasminogen activator. At 2–3 days after bulbectomy, there were degenerative changes in the olfactory epithelium. At 5–7 days after bulbectomy, we noted drastic differences in olfactory epithelium morphology between mice deficient in tissue plasminogen activator and wild-type mice (comparisons were made using findings from a previous study). The microvilli seemed to be normal and olfactory vesicles and receptor neuron dendrites were largely intact in the olfactory epithelium of mice deficient in tissue plasminogen activator.

Conclusion: The tissue plasminogen activator plasmin system may inhibit the regeneration of the olfactory epithelium in the early stages following neural injury.

Key words: Mouse; Microscopy, Electron, Transmission; Plasminogen Activators; Olfaction; Pathophysiology; Regeneration

Introduction

The olfactory epithelium consists of olfactory receptor neurons, supporting cells and basal cells. Throughout the vertebrate lifespan, there is continuous replacement of the olfactory receptor neurons, which regenerate from basal cells.[1] Olfactory receptor neurons also undergo replacement after neuronal injury. Many studies have examined the degeneration and regeneration of the olfactory epithelium following neuronal injury.[1,2] Our group has reported on the morphological changes of supporting cells following bulbectomy; these changes contribute to the regeneration of the olfactory epithelium.[3] However, many aspects of olfactory epithelium regeneration remain unclear, including the mechanisms involved, the molecular pathways and the morphology.

Several recent studies have revealed that tissue-type plasminogen activator is closely related to neuronal injury in the central and peripheral nervous system.[4] One report showed that tissue plasminogen activator was expressed in neuronal cells such as microglia and astrocytes, and that it played an important role in the central nervous system in response to excitotoxic injury.[5] Studies using 'knock-out' mice deficient in tissue plasminogen activator showed a decrease in neurotoxic effects in these mice, and neurons cultured from these mice were protected against hypoxia and oxidative stress.[6] Mice deficient in tissue plasminogen activator also showed reduced neural damage following focal cerebral ischaemia[7] and injury to the spinal cord.[8] Tissue plasminogen activator has been reported to be expressed in the olfactory bulb.[9] In that particular

Accepted for publication 4 January 2012

study, it was suggested that tissue plasminogen activator played a regulatory role in the development and maintenance of the olfactory system; however, no morphological changes were identified within the olfactory epithelium.

In order to provide evidence that tissue plasminogen activator is indeed involved in the development and maintenance of the olfactory system, it is necessary to show the associated morphological changes within the olfactory epithelium. The current study therefore examined the morphological changes of the olfactory epithelium before and after injury, using mice deficient in tissue plasminogen activator.

The results of this study suggest that tissue plasminogen activator is a regulator of supporting cell function and its absence may enhance regeneration of the olfactory epithelium after bulbectomy. To our knowledge, this is the first study to examine the olfactory epithelium of mice deficient in tissue plasminogen activator using transmission electron microscopy.

Materials and methods

Animals and surgery

This study used mice (12–16 weeks old) with tissue plasminogen activator deficiency.[10] These mice were originally derived from common, inbred laboratory mice type C57BL/6. All surgical procedures were carried out in accordance with the guidelines approved by the Jichi Medical University Animal Care and Concern Committee.

The mice were anaesthetised with 2.4 per cent isofluorane inhalation (180 ml/minute). After cutting the right olfactory nerve under a stereomicroscope, the right olfactory bulb was removed (bulbectomy) using vacuum aspiration with a fine stainless steel tube. The animals underwent morphological examination on days 1, 2, 3, 5 or 7 after the unilateral bulbectomy, with four mice per group (i.e. 20 mice in total). A control group was also established ($n = 4$); the mice in this group underwent a sham operation.

Tissue preparation for microscopy

The mice were perfused through the heart with a cold physiological saline solution, followed by 2 per cent paraformaldehyde and 2.5 per cent glutaraldehyde buffered with 0.1 M cacodylate solution (pH 7.4). Epithelial tissue from the nasal septum was carefully dissected and immersed in the same fixative for 12 hours. After washing with cold cacodylate buffer, the specimens were post-fixed with 1 per cent osmium tetroxide solution buffered with cacodylate solution for 2 hours on ice. Specimens were then treated with 0.5 per cent uranyl acetate for 2 hours at room temperature. This was followed by dehydration with an ascending ethanol series. The specimens were then embedded in an Epon mixture (TAAB Laboratories, Berks, UK). For light microscopy, Epon-embedded sections (0.5–0.7 μm thick) were stained with toluidine blue. For electron microscopy, ultrathin sections were mounted on a copper grid and stained with uranyl acetate and lead citrate. Sections were observed using a Jem-2000EX electron microscope (Tokyo, Japan).

Results

Light microscopy

Prior to bulbectomy, the free surface of the epithelium was covered with a faintly stained brush border of supporting cells, olfactory vesicles and mucus (Figure 1a). One day after bulbectomy, the olfactory vesicles appeared to be intact (Figure 1b). However, 2 days after bulbectomy, there were a reduced number of olfactory vesicles on the free surface of the epithelium (Figure 1c). Some cytoplasmic projections were also identified. In addition, numerous small, empty vesicles were present in the apical area of the supporting cells. Three days after bulbectomy, the olfactory vesicles were barely recognisable on the free surface of the epithelium, and a large number of cytoplasmic projections were observed within the brush borders (Figure 1d). Five days after bulbectomy, the cytoplasmic projections had disappeared from the free surface of the epithelium and olfactory vesicles were found there (Figure 1e). Seven days after bulbectomy, olfactory vesicles were found on the free surface of the epithelium (Figure 1f).

Electron microscopy

At baseline. Figure 2 shows electron micrographs of the intact olfactory epithelium of mice with tissue plasminogen activator deficiency, prior to bulbectomy. These micrographs reveal the free surface of the epithelium and the underlying olfactory receptor neurons and supporting cells. Ciliated olfactory vesicles extended above the free surface of the epithelium, and distinct, tight junctions were observed between the olfactory vesicles and the supporting cells. Microvilli were detected on the free surface of the supporting cells. The apical portion of the cells contained numerous rod-shaped mitochondria and membranous structures. A uniformly fine material was observed in some regions (Figure 2b) under transmission electron microscopy, but not under light microscopy.

One day after bulbectomy. The free surface of the olfactory epithelium from mice with tissue plasminogen activator deficiency exhibited a complex structure with many vacuoles located among the microvilli (Figure 3a and 3b). These vacuoles probably resulted from the degenerating cilia. Olfactory vesicles were overlaid with the degenerating microvilli and cilia. Figure 3c shows slight degeneration of the olfactory vesicles and degenerating cilia in the olfactory epithelium.

Two days after bulbectomy. The number of microvilli protruding from the supporting cell surfaces on the free surface of the olfactory epithelium had decreased

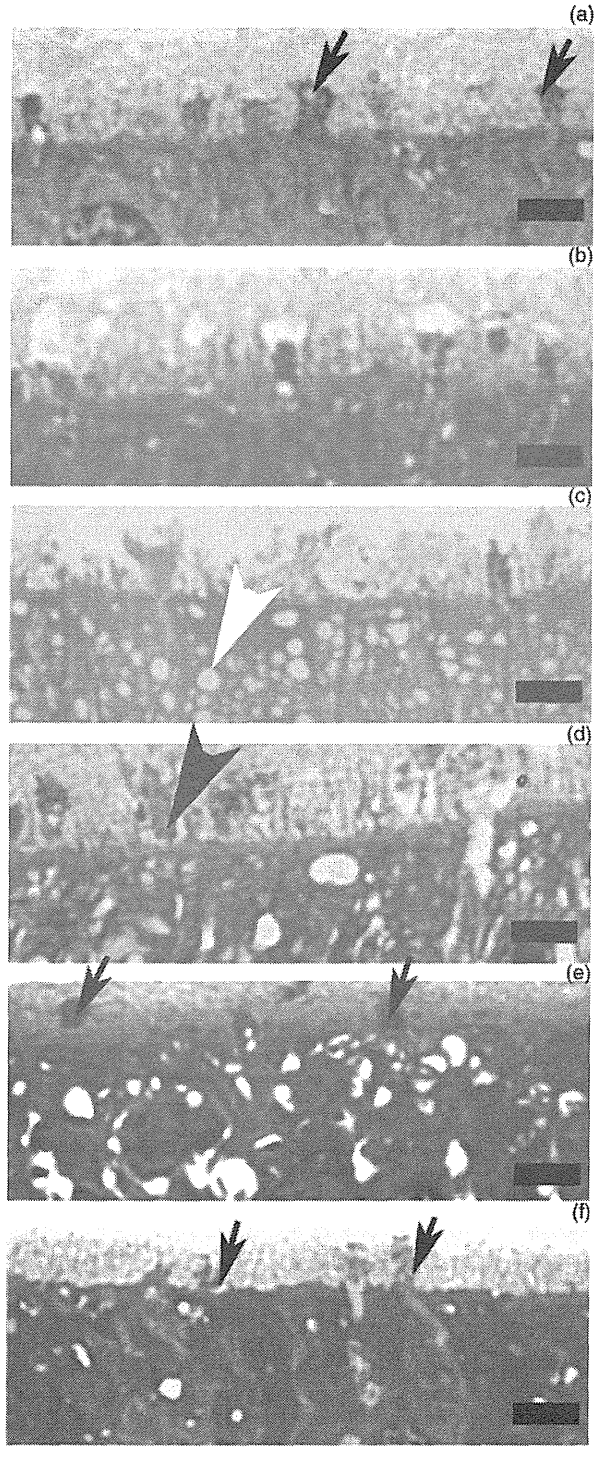

FIG. 1

Light micrographs of the olfactory epithelium. (a) Intact epithelium before bulbectomy. Olfactory vesicles (black arrows) can be seen on the free surface of the epithelium. (b) One day after bulbectomy. The staining of olfactory vesicles is unchanged. (c) Two days after bulbectomy. The number of olfactory vesicles on the free surface of the epithelium has declined. Numerous small, empty vesicles have appeared in the apical area (white arrowhead). (d) Three days after bulbectomy. Olfactory vesicles are barely recognisable. A large number of cytoplasmic projections (black arrowhead) are present in the brush borders. (e) Five days after bulbectomy. The cytoplasmic projections have disappeared and olfactory vesicles can again be seen (black arrows). (f) Seven days after bulbectomy. The epithelium is almost intact and olfactory vesicles can be seen (black arrows). (Bar = 3 μm)

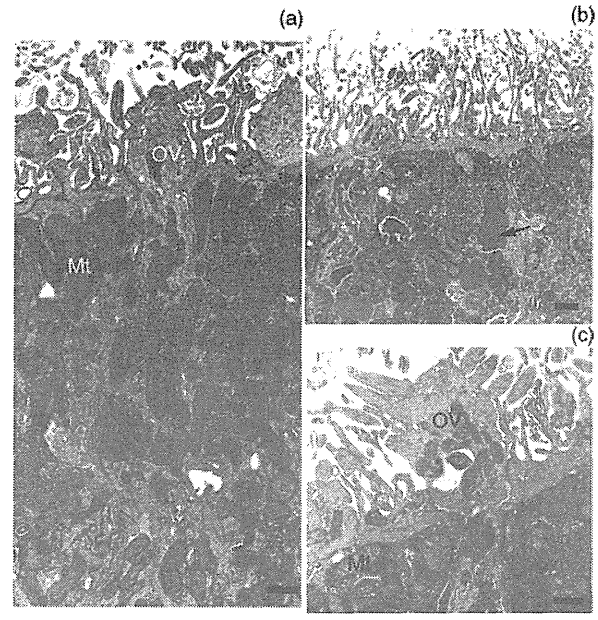

FIG. 2

Electron micrographs of the intact olfactory epithelium. (a) Ciliated olfactory vesicles can be seen. There are many rod-shaped mitochondria in the supporting cells. (b) A uniformly fine material is visible in the supporting cells (black arrow). (c) Ciliated olfactory vesicles and many rod-shaped mitochondria can be seen in the supporting cells. OV = olfactory vesicles; Mt = mitochondria (bar = 1 μm)

(Figure 4a). Instead of microvilli, we observed broad cytoplasmic projections containing undefined cytoplasmic organelles protruding into the luminal side (Figure 4a). In the cytoplasm of the supporting cells, the mitochondria were swollen, there was a decrease in the electron opacity and the cristae were obscure. There were numerous degenerating olfactory vesicles, with slight mitochondrial degeneration in the olfactory epithelium (Figure 4b). A uniformly fine material protruded onto the luminal surface of the olfactory epithelium in some regions (Figure 4a).

Three days after bulbectomy. The free surfaces of the olfactory epithelium were more prominent than those at 2 days after bulbectomy (Figure 5a). The cytoplasm of the supporting cells contained swollen and degenerated mitochondria, degenerated olfactory vesicles, and receptor neuron dendrites (Figure 5c). A large lamellar and smooth endoplasmic reticulum was evident within the cytoplasmic projections of the supporting cells in the microvilli (Figure 5b).

Five days after bulbectomy. Compared with observations at 3 days, we detected marked changes in the morphology of the olfactory epithelium 5 days after bulbectomy. Morphologically, the olfactory epithelium seemed almost completely recovered. The olfactory vesicles and receptor neuron dendrites were nearly intact (Figure 6a and 6b).

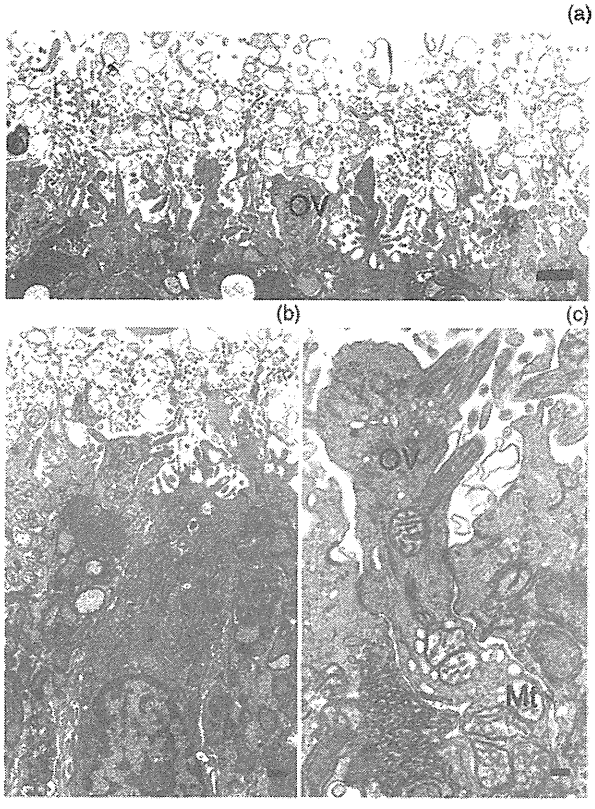

FIG. 3

Electron micrographs of the olfactory epithelium 1 day after bulbectomy. (a) & (b) The thickness of the microvilli from supporting cells has increased. There are many vacuoles derived from the degenerating cilia (bar = 1 μm). (c) Slight degeneration of the olfactory vesicles can be observed (bar = 200 nm). OV = olfactory vesicles; Mt = mitochondria

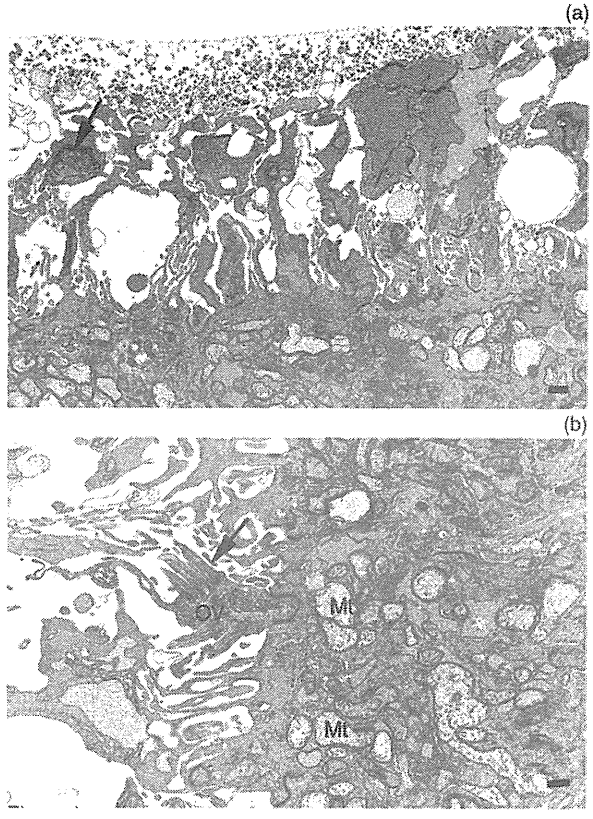

FIG. 4

Electron micrographs of the olfactory epithelium 2 days after bulbectomy. (a) Only a small number of microvilli and broad cytoplasmic projections can be seen. Some of the cytoplasmic projections contain unidentified cell organelles (black arrow). Materials with a uniform appearance have protruded into the luminal side (white arrow) (bar = 1 μm). (b) The mitochondria are swollen. The electron opacity of mitochondria has decreased and cristae are obscure. Olfactory vesicles with partially degenerated mitochondria (black arrow) can be observed (bar = 200 nm). OV = olfactory vesicles; Mt = mitochondria

Seven days after bulbectomy. In order to determine the morphological changes in the olfactory epithelium of mice deficient in tissue plasminogen activator, we compared the olfactory epithelium of these mice with that of wild-type mice at 7 days after bulbectomy (using findings from our previous study). In mice with tissue plasminogen activator deficiency (Figure 7a and 7b), the morphological features of the olfactory epithelium were similar to those of 'intact mice' (i.e. the wild-type mice that underwent the sham operation). Olfactory vesicles and receptor neuron dendrites were visible and showed almost complete morphological recovery. The smooth endoplasmic reticulum and mitochondria in the cytoplasm of the apical portion of the supporting cells were nearly intact.

Discussion

Degeneration of the olfactory epithelium after neuronal injury is a significant clinical problem because it leads to irreversible olfactory disorders. Several experimental studies have reported on this problem, but many aspects remain unclear. Our recent investigations have focused on tissue plasminogen activator as a possible molecule involved in the recovery of olfactory epithelium.

The tissue plasminogen activator plasmin system is well understood. Plasmin is converted from the zymogen plasminogen by tissue plasminogen activator or urokinase-type plasminogen activator, and can degrade the extracellular matrix. These proteolytic activities of plasmin are involved in neuronal death.[4–6] Fibrinolytic system components play important roles in the nervous system.[4] In addition to acting as a fibrinolytic agent, it has been suggested that tissue plasminogen activator plays an important role in the brain. For instance, tissue plasminogen activator may interact with the N-methyl-D-aspartate receptor complex,[11] thereby mediating microglial activation.[12] Furthermore, mice deficient in tissue plasminogen activator showed reduced blood–brain barrier injury following focal cerebral ischaemia.[13]

The potential role of the tissue plasminogen activator plasmin system in the olfactory epithelium has been demonstrated indirectly. Non-integrin laminin receptor precursor protein is expressed in the olfactory stem and progenitor cells.[14] Matrix metalloproteinases 9 and 2

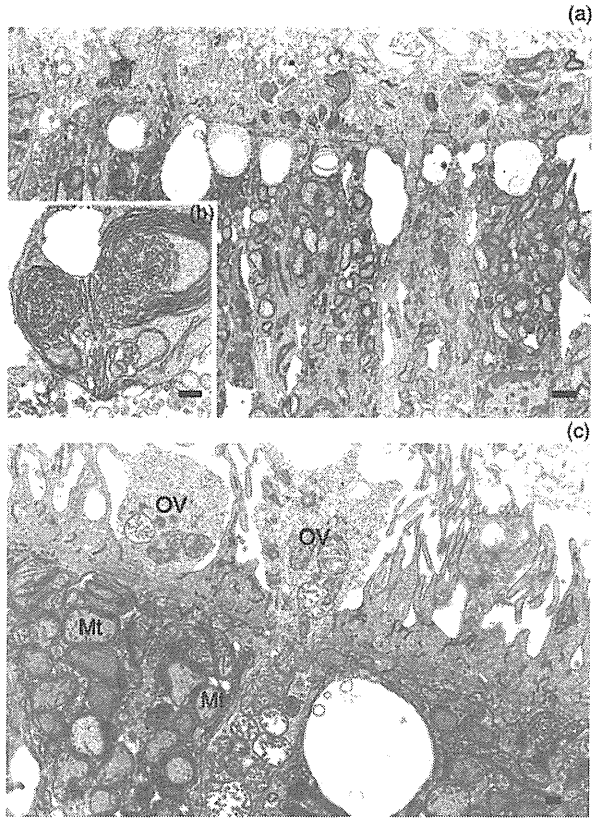

FIG. 5

Electron micrographs of the olfactory epithelium 3 days after bulbectomy. (a) Only a small number of microvilli and broad cytoplasmic projections are present (bar = 1 μm). (b) The projections of the supporting cells contain smooth endoplasmic reticulum (bar = 200 nm). (c) The olfactory vesicles have almost disappeared. The smooth endoplasmic reticulum and the degenerating mitochondria are closely linked (bar = 200 nm). OV = olfactory vesicles; Mt = mitochondria

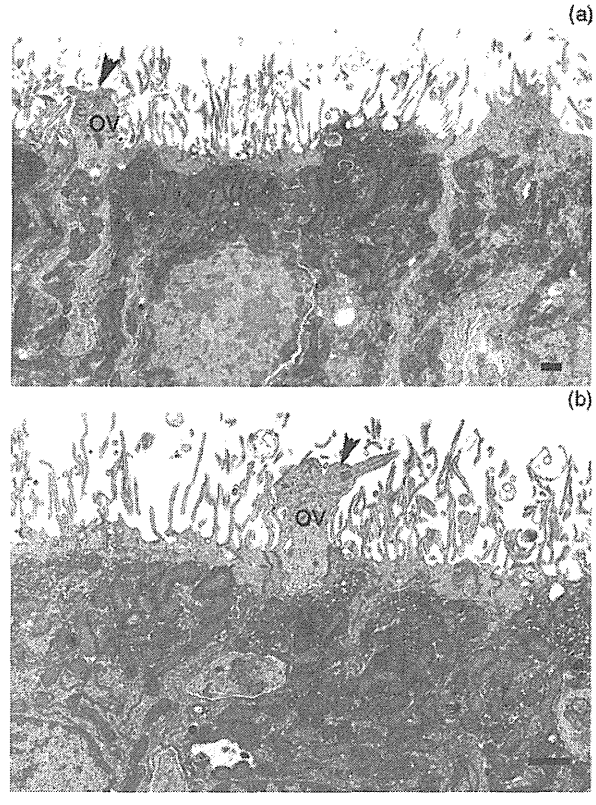

FIG. 6

Electron micrographs of the olfactory epithelium 5 days after bulbectomy. (a) Near-normal microvilli and mitochondria are present. Olfactory vesicles and receptor neuron dendrites are visible (black arrowhead). (b) Olfactory vesicles and receptor neuron dendrites are visible (black arrowhead). OV = olfactory vesicles (bar = 1 μm)

are expressed in the olfactory epithelium,[15,16] and their expression increases in the olfactory epithelium[15,17] and olfactory bulb.[18] Plasmin may play a role in degrading laminin and activating matrix metalloproteinases. Therefore, we hypothesised that tissue plasminogen activator and other fibrinolytic factors may be involved in the continuous neurogenesis cell proliferation, migration and/or differentiation seen within the olfactory epithelium.

In this novel study, we examined the olfactory epithelium of mice deficient in tissue plasminogen activator following bulbectomy, using light microscopy and transmission electron microscopy. We compared our findings with those of our previous study using wild-type mice treated in the same way.[3] As the mice deficient in tissue plasminogen activator were derived from C57BL/6 mice, any differences between these types of mice should reflect the function of tissue plasminogen activator in the olfactory epithelium.

For our light microscopic observations, we stained sections of plastic-embedded material (0.5–0.7 μm thick) with toluidine blue. At 0–2 days after bulbectomy, we found that the morphological changes at the free surface of the olfactory epithelium were similar for both wild-type mice and mice deficient in tissue plasminogen activator. At 5–7 days after bulbectomy, the olfactory vesicles at the free surface of the epithelium were barely recognisable in wild-type mice, and numerous cytoplasmic projections were observed within the brush borders in these mice.[3] In fact, it is often reported that the olfactory neurons of wild-type mice almost vanish at 5–7 days after bulbectomy.[1–3,15,17] However, in the olfactory epithelium of mice deficient in tissue plasminogen activator, olfactory vesicles were recognisable, and the cytoplasmic projections had disappeared.

Transmission electron microscopy observations of the pre-bulbectomy olfactory epithelium showed marked morphological differences in the supporting cells of mice deficient in tissue plasminogen activator, compared with those of wild-type mice. We also found that the prevalence of an unknown, uniformly fine material within the supporting cells, indicative of phagocytic ability,[2] had decreased in mice deficient in tissue plasminogen activator. This apparent decline in terms of phagocytic ability was not seen in the supporting cells of wild type mice. This suggests that the tissue plasminogen activator plasmin system regulates olfactory epithelium regeneration.

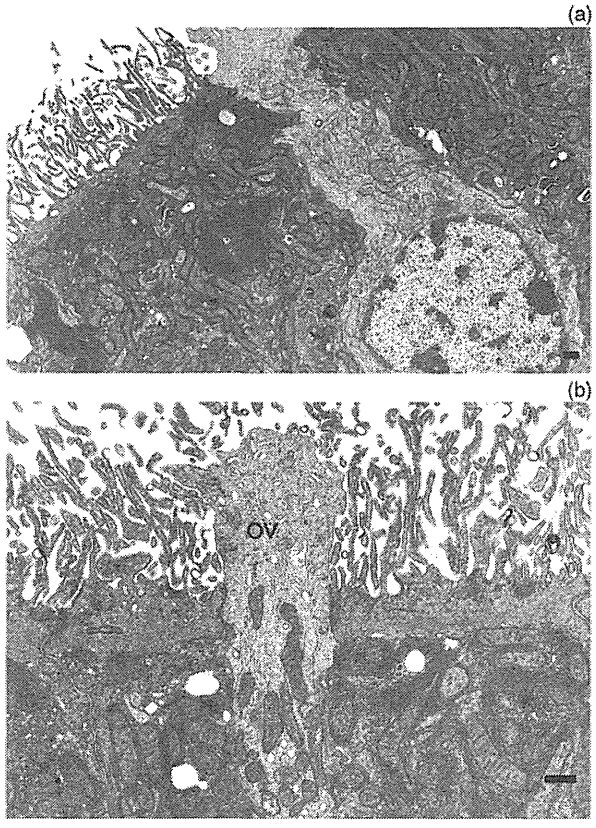

FIG. 7

Electron micrographs of the olfactory epithelium 7 days after bulbectomy. (a) The olfactory epithelium has a near-normal appearance. (b) Normal olfactory vesicles and receptor neuron dendrites are visible. OV = olfactory vesicles

At 5 days after bulbectomy, the morphological features of the olfactory epithelium in mice deficient in tissue plasminogen activator were similar to those prior to bulbectomy. We found numerous intact olfactory vesicles and almost fully recovered supporting cells in the olfactory epithelium.

- **The olfactory epithelium of mice deficient in tissue plasminogen activator was examined using light and transmission electron microscopy**
- **An unknown, uniformly fine material was seen in epithelial supporting cells pre-bulbectomy**
- **The olfactory neurons of wild-type mice are reported to almost vanish 5–7 days after bulbectomy**
- **The olfactory neurons of mice deficient in tissue plasminogen activator were regenerating at 5–7 days after bulbectomy**
- **The tissue plasminogen activator plasmin system may inhibit olfactory epithelium regeneration following neural injury**

To further clarify the morphological changes, we compared the olfactory epithelium of wild-type (intact) mice with mice deficient in tissue plasminogen activator 7 days after bulbectomy. In the mice deficient in tissue plasminogen activator, the morphological features of the supporting cells were similar to those of the wild-type mice. However, the olfactory vesicles and receptor neuron dendrites were visible in mice deficient in tissue plasminogen activator, but not in wild-type mice. Furthermore, the olfactory epithelium was still in a severe degenerative state in the wild-type mice.

The findings of this study suggest that the olfactory receptor neurons regenerate earlier in mice with tissue plasminogen activator deficiency than in wild-type mice. It is hypothesised that the tissue plasminogen activator plasmin system might play an inhibitory role in the regeneration of the olfactory epithelium following bulbectomy.

In clinical settings, tissue plasminogen activator has been used in fibrinolytic therapy for acute myocardial infarction[19] and cerebral infarction.[20] Our results provide evidence that the suppression of tissue plasminogen activator activity in the olfactory epithelium may improve functional recovery following olfactory tract injury, by affecting the degeneration and regeneration of the olfactory epithelium. These findings could lead to new therapeutic strategies for the treatment of olfactory disorders.

Acknowledgments

We would like to thank T Ohmori, A Ishiwata, Y Kashiwakura, Y Noda, K Okada and S Ueshima for their advice and helpful discussion. This study was supported by an official annual grant from Jichi Medical University School of Medicine.

References

1 Graziadei PP, Graziadei GA. Neurogenesis and neuron regeneration in the olfactory system of mammals. I. Morphological aspects of differentiation and structural organization of the olfactory sensory neurons. *J Neurocytol* 1979;**8**:1–18
2 Suzuki Y. Fine structural aspects of apoptosis in the olfactory epithelium. *J Neurocytol* 2004;**33**:693–702
3 Makino N, Ookawara S, Katoh K, Ohta Y, Ichikawa M, Ichimura K. The morphological change of supporting cells in the olfactory epithelium after bulbectomy. *Chem Senses* 2009; **34**:171–9
4 Nagai N, Matsuo O. Roles of fibrinolytic system components in the nervous system. *Pathophysiology* 2010;**17**:141–7
5 Siao CJ, Fernandez SR, Tsirka SE. Cell type-specific roles for tissue plasminogen activator released by neurons or microglia after excitotoxic injury. *J Neurosci* 2003;**23**:3234–42
6 Nagai N, Yamamoto S, Tsuboi T, Ihara H, Urano T, Takada Y *et al.* Tissue-type plasminogen activator is involved in the process of neuronal death induced by oxygen-glucose deprivation in culture. *J Cereb Blood Flow Metab* 2001;**21**:631–4
7 Lee SR, Lok J, Rosell A, Kim HY, Murata Y, Atochin D *et al.* Reduction of hippocampal cell death and proteolytic responses in tissue plasminogen activator knockout mice after transient global cerebral ischemia. *Neuroscience* 2007;**150**:50–7
8 Abe Y, Nakamura H, Yoshino O, Oya T, Kimura T. Decreased neural damage after spinal cord injury in tPA-deficient mice. *J Neurotrauma* 2003;**20**:43–57
9 Thewke DP, Seeds NW. Expression of hepatocyte growth factor/scatter factor, its receptor c-met, and tissue-type

plasminogen activator during development of the murine olfactory system. *J Neurosci* 1996;**16**:6933–44
10 Carmeliet P, Schoonjans L, Kieckens L, Ream B, Degen J, Bronson R *et al.* Physiological consequences of loss of plasminogen activator gene function in mice. *Nature* 1994; **368**:419–24
11 Nicole O, Docagne F, Ali C, Margaill I, Carmeliet P, MacKenzie ET *et al.* The proteolytic activity of tissue-plasminogen activator enhances NMDA receptor-mediated signaling. *Nat Med* 2001;**7**: 59–64
12 Gravanis I, Tsirka SE. Tissue plasminogen activator and glial function. *Glia* 2005;**49**:177–83
13 Tsuji K, Aoki T, Tejima E, Arai K, Lee SR, Atochin DN *et al.* Tissue plasminogen activator promotes matrix metalloproteinase-9 upregulation after focal cerebral ischemia. *Stroke* 2005; **36**:1954–9
14 Jang W, Kim KP, Schwob JE. Nonintegrin laminin receptor precursor protein is expressed on olfactory stem and progenitor cells. *J Comp Neurol* 2007;**502**:367–81
15 Costanzo RM, Perrino LA, Kobayashi M. Response of matrix metalloproteinase-9 to olfactory nerve injury. *Neuroreport* 2006;**17**:1787–91
16 Tsukatani T, Fillmore HL, Hamilton HR, Holbrook EH, Costanzo RM. Matrix metalloproteinase expression in the olfactory epithelium. *Neuroreport* 2003;**14**:1135–40
17 Costanzo RM, Perrino LA. Peak in matrix metaloproteinases-2 levels observed during recovery from olfactory nerve injury. *Neuroreport* 2008;**19**:327–31
18 Bakos SR, Schwob JE, Costanzo RM. Matrix metalloproteinase-9 and -2 expression in the olfactory bulb following methyl bromide gas exposure. *Chem Senses* 2010;**35**:655–61
19 Llevadot J, Giugliano RP, Antman EM. Bolus fibrinolytic therapy in acute myocardial infarction. *JAMA* 2001;**286**:442–9
20 Fugate JE, Giraldo EA, Rabinstein AA. Thrombolysis for cerebral ischemia. *Front Neurol* 2010;**1**:139

Address for correspondence:
Dr Nobuko Makino,
Department of Otolaryngology – Head and Neck Surgery,
Jichi Medical University School of Medicine,
3311-1 Yakushiji,
Shimotsuke, Tochigi 329-0498, Japan

Fax: +81 285 44 5547
E-mail: n-makino@jichi.ac.jp

Dr N Makino takes responsibility for the integrity of the content of the paper
Competing interests: None declared

Cell Stem Cell
Brief Report

Il2rg Gene-Targeted Severe Combined Immunodeficiency Pigs

Shunichi Suzuki,[1] Masaki Iwamoto,[3] Yoriko Saito,[4] Daiichiro Fuchimoto,[1] Shoichiro Sembon,[1] Misae Suzuki,[1] Satoshi Mikawa,[2] Michiko Hashimoto,[3] Yuki Aoki,[4] Yuho Najima,[4] Shinsuke Takagi,[4] Nahoko Suzuki,[4] Emi Suzuki,[5] Masanori Kubo,[6] Jun Mimuro,[7] Yuji Kashiwakura,[7] Seiji Madoiwa,[7] Yoichi Sakata,[7] Anthony C.F. Perry,[8] Fumihiko Ishikawa,[4,*] and Akira Onishi[1,*]

[1]Transgenic Animal Research Center
[2]Animal Genome Research Unit
National Institute of Agrobiological Sciences, Tsukuba, Ibaraki 305-0901, Japan
[3]Prime Tech Ltd., Tsuchiura, Ibaraki 300-0841, Japan
[4]Research Unit for Human Disease Model, RIKEN Research Center for Allergy and Immunology, Yokohama, Kanagawa 230-0045, Japan
[5]Laboratory of Mammalian Molecular Embryology, RIKEN Research Center for Developmental Biology, Kobe 650-0047, Japan
[6]Center for Animal Disease Control and Prevention, National Institute of Animal Health, Tsukuba, Ibaraki 305-0856, Japan
[7]Division of Cell and Molecular Medicine, Center for Molecular Medicine, Jichi Medical University, Tochigi-ken 329-0498, Japan
[8]Laboratory of Mammalian Molecular Embryology, Department of Biology and Biochemistry, University of Bath, Bath BA2 7AY, UK
*Correspondence: f_ishika@rcai.riken.jp (F.I.), onishi@affrc.go.jp (A.O.)
DOI 10.1016/j.stem.2012.04.021

SUMMARY

A porcine model of severe combined immunodeficiency (SCID) promises to facilitate human cancer studies, the humanization of tissue for xenotransplantation, and the evaluation of stem cells for clinical therapy, but SCID pigs have not been described. We report here the generation and preliminary evaluation of a porcine SCID model. Fibroblasts containing a targeted disruption of the X-linked interleukin-2 receptor gamma chain gene, *Il2rg*, were used as donors to generate cloned pigs by serial nuclear transfer. Germline transmission of the *Il2rg* deletion produced healthy *Il2rg*$^{+/-}$ females, while *Il2rg*$^{-/Y}$ males were athymic and exhibited markedly impaired immunoglobulin and T and NK cell production, robustly recapitulating human SCID. Following allogeneic bone marrow transplantation, donor cells stably integrated in *Il2rg*$^{-/Y}$ heterozygotes and reconstituted the *Il2rg*$^{-/Y}$ lymphoid lineage. The SCID pigs described here represent a step toward the comprehensive evaluation of preclinical cellular regenerative strategies.

The common gamma chain, IL2RG, is an IL-2 receptor subunit (Takeshita et al., 1992) shared by IL-4, IL-7, IL-9, IL-15, and IL-21 receptors (Kondo et al., 1993; Noguchi et al., 1993a; Russell et al., 1993; Giri et al., 1994; Kimura et al., 1995; Asao et al., 2001). IL2RG is present in T, NK, NKT, and dendritic cells (Ishii et al., 1994) and plays an essential role in lymphoid development by activating, through its cytoplasmic domain, Janus kinase 3 (Nakamura et al., 1994; Nelson et al., 1994, 1997).

Mammalian *IL2RG* orthologs are typically located on the X chromosome; in humans, *IL2RG* mutations result in X-linked severe combined immunodeficiency (XSCID) in which T and NK cells are absent or profoundly reduced in number, while B cells are numerically normal (or increased) but functionally impaired (Noguchi et al., 1993b; Leonard, 1996; Fischer et al., 1997). Gene-targeted mice lacking *Il2rg* also exhibit immunological defects (Cao et al., 1995; Ohbo et al., 1996) including the ablation of NK cell activity. NOD/SCID/*Il2rg*^{null}, NOG, and *Rag2*^{null}/*Il2rg*^{null} mice permit the functional reconstitution of human hematopoietic and immune systems following the injection of purified human hematopoietic stem cells (Traggiai et al., 2004; Ishikawa et al., 2005; Shultz et al., 2005). Unfortunately, phenotypic differences exist between XSCID humans and *Il2rg* null mice, including a pronounced numerical B cell reduction in the latter. Two dog breeds develop SCID caused by *Il2rg* mutations (Felsburg et al., 1999; Perryman, 2004), but dogs are poorly characterized research models.

In contrast, the pig more closely resembles humans regarding anatomy, hematology, physiology, size, and longevity. By enabling long-term follow-up, pig models will permit the evaluation of human cancer and stem cell transplantation over clinically relevant time frames. We here describe disruption of the porcine *Il2rg* gene to generate SCID pigs, their phenotypic characterization, and proof-of-principle transplantation studies.

A conventional positive-negative selection *Il2rg* gene targeting vector (TV) (Figure S1A) enabled the functional inactivation of porcine *Il2rg* by removing exon 6 (Kanai et al., 1999). Following fetal fibroblast transfection, selection, and PCR screening, 1 of 3 TV-targeted cell lines was expanded for nuclear transfer (Table S1). Even after screening, PCR-positive colonies often contain a substantial proportion of nontargeted cells (not shown) that would result in a corresponding proportion of nontargeted cloned pigs following nuclear transfer. To ensure that all clones harbored a targeted *Il2rg* locus, we adopted a serial cloning strategy. Nine embryonic day 35 (E35) or E39 nuclear transfer embryos were collected and screened by PCR and Southern blotting. PCR (not shown) and Southern blotting (Figure S1B) revealed that six contained the genomic configuration predicted for a single-targeted *Il2rg* allele. Fibroblasts were cultured from one targeted embryo and used in secondary nuclear transfer to

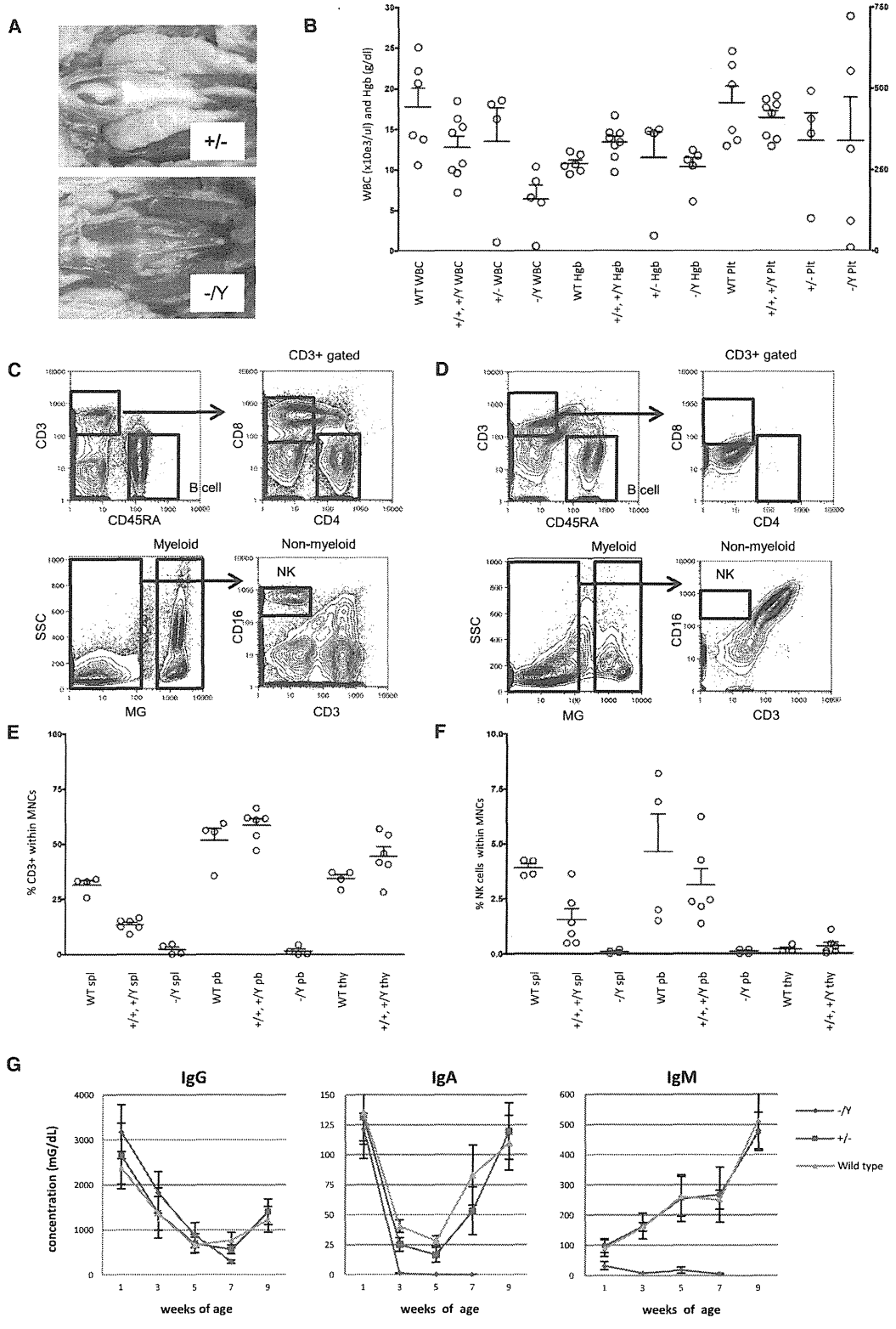
A
+/-
-/Y
B
WBC (x10e3/ul) and Hgb (g/dl)
Plt (x10e3/ul)
WT WBC
+/+, +/Y WBC
+/- WBC
-/Y WBC
WT Hgb
+/+, +/Y Hgb
+/- Hgb
-/Y Hgb
WT Plt
+/+, +/Y Plt
+/- Plt
-/Y Plt
C
CD3+ gated
CD3
CD45RA
B cell
CD8
CD4
Myeloid
Non-myeloid
SSC
MG
NK
CD16
CD3
D
CD3+ gated
CD3
CD45RA
B cell
CD8
CD4
Myeloid
Non-myeloid
SSC
MG
NK
CD16
CD3
E
% CD3+ within MNCs
WT spl
+/+, +/Y spl
-/Y spl
WT pb
+/+, +/Y pb
-/Y pb
WT thy
+/+, +/Y thy
F
% NK cells within MNCs
WT spl
+/+, +/Y spl
-/Y spl
WT pb
+/+, +/Y pb
-/Y pb
WT thy
+/+, +/Y thy
G
IgG
IgA
IgM
concentration (mG/dL)
weeks of age
-/Y
+/-
Wild type

produce 31 cloned F_0 piglets; all were females heterozygously targeted at their *Il2rg* genes as judged by PCR (not shown) and Southern blotting (Figure S1C).

Fourteen of the 31 were stillborn and 3 of the 17 live-born died neonatally of unknown cause(s) (Table S1). Ten survivors died from pneumonia and severe arthritis (five were euthanized) between postnatal day 7 (P7) and P70. The remaining four (#5, 9, 15 and 20) survived for >1 year.

Stillborn and neonatal fatalities often had spleens with hypoplastic lymphoid aggregations (Figure S1D). Most (24/31, 77%) had undetectable or severely hypoplastic thymi (Figure S1E and Table S2). F_0 clones that died within 10 weeks also lacked detectable thymi and had few, if any, T cells either in their spleens or circulating (Figures S1F and S1G). In contrast, levels of $CD4^+$ and $CD8^+$ T cells in four long-lived F_0 lines were comparable to those of WT controls. Analysis of peripheral blood (PB) mononuclear cell (PBMC) RNA corroborated this: *Il2rg, CD4,* and *CD8* transcript levels were reduced in athymic $Il2rg^{+/-}$ clones that perished relative to respective levels in long-lived clones and WT controls (Figure S1H).

Thus, most $Il2rg^{+/-}$ clones exhibited SCID-like phenotypes, albeit that they had one WT allele. We attributed this high proportion to aberrant X-inactivation, a previously observed epigenetic cloning phenotype (Senda et al., 2004; Nolen et al., 2005; Jiang et al., 2008). However, epigenetic cloning phenotypes are corrected by germline transmission (Shimozawa et al., 2002). To confirm this and isolate the $Il2rg^{+/-}$ phenotype, we analyzed progeny derived by fertilization from $Il2rg^{+/-}$ cloned female #9.

Female $Il2rg^{+/-}$ #9 inseminated with WT sperm produced 19 F_1 (12 m, 7 f) offspring, and of these F_1 offspring, two $Il2rg^{+/-}$ females produced 21 F_2 (13 m, 8 f) when inseminated with WT sperm. Autopsies of representative F_1 and F_2 progeny revealed that, as expected, all $Il2rg^{-/Y}$ males had undetectable thymi, whereas $Il2rg^{+/-}$ females had thymi of normal size (Figure 1A and Table S3).

Hematological parameters in PB exhibited a significantly ($p = 0.0041$) reduced white blood cell (WBC) count in F_1 $Il2rg^{-/Y}$ males ($6.4 \pm 1.6 \times 10^3/\mu l$, $n = 5$) compared to WT controls ($17.8 \pm 2.3 \times 10^3/\mu l$, $n = 6$), while hemoglobin levels and platelet counts were unaffected (Figure 1B). F_1 $Il2rg^{+/-}$ females and WT littermates yielded comparable PB T, NK, and B cell numbers, indicative of intact acquired and innate immunity (Figures 1C, 1E, and 1F). In contrast, $Il2rg^{-/Y}$ males harbored significantly reduced PB T cells ($Il2rg^{-/Y}$ males, $1.5\% \pm 1.0\%$; $Il2rg^{+/Y}$ males, $57.3\% \pm 4.3\%$; $n = 4$ each, $p < 0.0001$) and NK cells ($Il2rg^{-/Y}$ males, $0.1\% \pm 0.1\%$; $Il2rg^{+/Y}$ males, $3.6\% \pm 1.1\%$; $n = 4$ each, $p = 0.0162$) (Figures 1D, 1E, and 1F). In proportion to the PB reductions, $Il2rg^{-/Y}$ spleens exhibited significant numerical reductions of T cells ($Il2rg^{-/Y}$ males, $2.3\% \pm 1.1\%$; $Il2rg^{+/Y}$ males, $13.0\% \pm 1.4\%$; $n = 4$ each, $p = 0.0011$) and NK cells ($Il2rg^{-/Y}$ males, $0.1\% \pm 0.0\%$; $Il2rg^{+/Y}$ males, $0.8\% \pm 0.2\%$; $n = 4$ each, $p = 0.0162$) (Figures 1E and 1F). B cells and myeloid cells accounted for the majority of $CD45^+$ leukocytes in $Il2rg^{-/Y}$ males, indicating that their immune deficiency was limited to T and NK cell lineages. The presence in $Il2rg^{-/Y}$ males of $CD33^+$ myeloid cells with both mononuclear and polynuclear properties suggests the differentiation of both granulocyte lineages and antigen-presenting cells, including monocytes and dendritic cells (Figures 1C and 1D).

We next evaluated humoral immune status in *Il2rg*-targeted pigs (Figure 1G). Serum IgG and IgA levels were high at 1 week (P7) and decreased gradually from 3 to 5 weeks in $Il2rg^{-/Y}$ (males), WT littermates, and $Il2rg^{+/-}$ female controls. After 7 weeks, IgG and IgA levels re-elevated in WT controls, while levels of both remained low in $Il2rg^{-/Y}$ males. Serum IgM was low at 1 week and increased gradually in controls but remained low in $Il2rg^{-/Y}$ males. Because both IgG and IgA at 1 week of age are entirely transferred via the colostrum in pigs, these results indicate that there had been no de novo Ig production in $Il2rg^{-/Y}$ males after weaning at 4 weeks. Impaired antibody production by $Il2rg^{-/Y}$ B cells is likely due to the absence of critical $CD4^+$ T helper cells. Consistent with their impaired immunity, all F_1 $Il2rg^{-/Y}$ males became systemically ill in the conventional housing conditions used, while F_1 $Il2rg^{+/-}$ females appeared healthy.

Collectively, this shows that when produced by conventional breeding, $Il2rg^{-/Y}$ F_1 males, but not $Il2rg^{+/-}$ females, present SCID phenotypes. SCID-like phenotypes observed in many $Il2rg^{+/-}$ female clones are attributable to aberrant, nonrandom X-inactivation during somatic cell cloning. Following germline transmission, *Il2rg*-targeted phenotypes resembled those of X-linked SCID in other species, with greatly reduced T and NK cell development and function (Cao et al., 1995; Puck et al., 1987). *Il2rg*-targeted pigs harbor B cells and thereby recapitulate human XSCID more closely than do *Il2rg*-targeted mice.

We next performed proof-of-principle allogeneic transplantation experiments using *Il2rg*-targeted pigs as recipients. Preliminary conditioning with orally administered fludarabine and busulfan produced significantly decreased WBC and platelet counts (not shown), which might promote the engraftment of transplanted cells. However, 2 of 6 $Il2rg^{-/Y}$ males died within 2 weeks postadministration, suggesting that the regimen was lethal for some piglets. Bone marrow (BM) cells from WT siblings were intravenously transplanted to four P11-12 $Il2rg^{-/Y}$ males with (#113, #115) or without (#605, #610) conditioning. Ubiquitously GFP-expressing (#184) BM cells (Watanabe et al., 2005)

Figure 1. Phenotypes of F_1 and F_2 Progeny Derived from $Il2rg^{+/-}$ Clone #9 by Germline Transmission

(A) Thymic phenotype in an $Il2rg^{+/-}$ female at 10 weeks and an $Il2rg^{-/Y}$ male at 9 weeks.

(B) Peripheral blood (PB) white blood cell (WBC), hemoglobin (Hgb), and platelet count (Plt) at 2 months of age in WT controls, $Il2rg^{+/+}$ female littermates, $Il2rg^{+/-}$ female littermates, and $IL2rg^{-/Y}$ males.

(C) Identification of acquired and innate immune subsets in an $Il2rg^{+/+}$ female by surface phenotype of $CD45RA^+CD3^-$ B cells, $CD3^+CD4^+$ T cells, $CD3^+CD8^+$ T cells, and $CD3^-CD16^+$ NK cells among the nonmyeloid fraction and myeloid cells.

(D) Analysis as for (C), but of an $IL2rg^{-/Y}$ male.

(E) Proportion of $CD3^+$ T cells in the spleen (spl), PB, and thymus (thy) in control $Il2rg^{+/+}$ females and male $Il2rg^{+/Y}$ littermates and nonlittermates (WT).

(F) Analysis as for (E), except showing the proportion of $CD3^-CD16^+$ NK cells.

(G) Changes with time postpartum in serum IgG (left), IgA (middle), and IgM levels. All error bars indicate SEM. See also Figure S1 and Tables S1–S3.

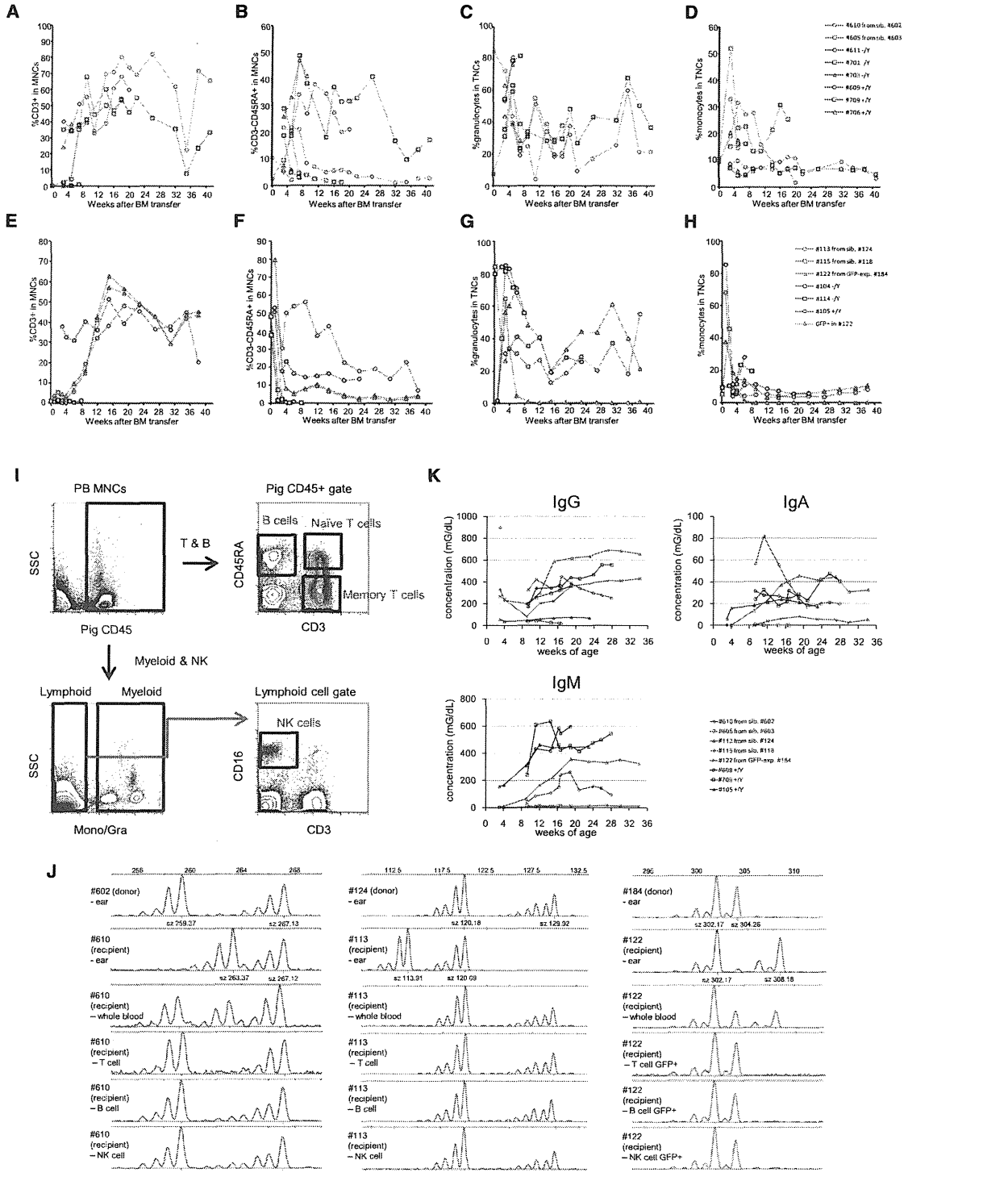

Figure 2. Allogeneic Bone Marrow Transfer into *Il2rg*$^{-/Y}$ Males

(A–H) Flow cytometric quantification of each subtype of leukocytes in *Il2rg*$^{-/Y}$ males (red lines) at different times after BM transfer. Controls are WT littermates (blue lines) and *Il2rg*$^{-/Y}$ males (black lines) without BM transfer. (A)–(D) correspond to BMT without conditioning, the case for #605 and #610. (E)–(H) correspond to BMT with conditioning, the case for #105, #113, and #122. (A) and (E) show the proportion of CD3$^+$ T cells in PB at different times after BM transfer. (B) and (F) show proportion of CD45RA$^+$CD3$^-$ B cells in PB at different times after BM transfer. (C) and (G) show proportion of granulocytes in PB at different times after BM transfer. (D) and (H) show proportion of monocytes in PB at different times after BM transfer.

were transferred to a *Il2rg*$^{-/Y}$ male (#122) with conditioning. Recipient #115 died 15 days after BM transfer (BMT), possibly due to conditioning toxicity, and recipient #605 died of presumptive pneumonia (not shown) 140 days posttransplantation; nevertheless, it survived longer than *Il2rg*$^{-/Y}$ controls without BMT, which died within 54 days. The remaining three recipients have survived >516 days (#610) and >321 days (#113 and #122) posttransplantation, with PB T cell populations exhibiting similar dynamics (Figures 2A and 2E); T cell counts increased ~6 weeks posttransplantation and remained high. Following early variability, PB B cell counts equilibrated at detectably low levels. The exception was #113, in which B cell counts were clearly higher than those of WT controls until 16 weeks posttransplantation, gradually decreasing thereafter to a level comparable with other recipients (Figures 2B and 2F). Compared to WT controls, recipient #610 PB contained similar T cell counts and a diminished but substantial number of B and NK cells 42 weeks posttransplantation (Figures 2A, 2B, and 2I). Similar profiles were observed in #113 and 122 (Figures 2E and 2F; not shown for NK). Surviving recipients and WT littermates had comparable granulocyte and monocyte numbers (Figures 2C, 2D, 2G, and 2H).

The provenance of immune cells in surviving recipients was examined by microsatellite marker analysis of genomic DNA from the ear, whole blood, and sorted T, B, and NK cells. GFP fluorescence of immune cells was also detected in the case of #122 (Figures 2E–2H and 2J). Lymphoid lineages were totally of donor origin in all recipients. Myeloid lineages were mainly of donor origin in #113 and of mixed donor/host origin in #122 and #610. Thus, our conditioning regimen enabled donor-derived myeloid lineage reconstitution in #113, but not #122. All surviving recipient PB contained IgG, IgA, and IgM (Figure 2K), albeit at varying levels, strongly suggesting that humoral immunity had been reconstituted and that donor-derived recipient B cells produced antibodies. Thus, allogeneic BM transplantation to *Il2rg*$^{-/Y}$ SCID pigs reproducibly resulted in enduring functional donor cell engraftment and reconstituted acquired immunity.

Assuming that the allogeneic model reported here reflects the behavior of cells transplanted from different species, SCID pigs promise to become a valuable tool in xenogeneic transplantation studies of human stem cells, such as hematopoietic, embryonic, and induced pluripotent stem cells (Takahashi et al., 2007). In particular, they promise to serve as platforms for the evaluation of therapeutic outcomes over several years, possibly after further genetic manipulation such as disruption of recombination activating genes 1 or 2 (*Rag1*, *Rag2*), which play critical roles in both cellular and humoral immunity (Shinkai et al., 1992) and may facilitate efficient human stem cell engraftment. Preliminary xenotransplantation of human BM cells to porcine *Il2rg*$^{-/Y}$ recipients in the absence of preconditioning permitted limited engraftment, underscoring the importance of further genetic manipulation, and optimized preconditioning (not shown). The porcine SCID model described here therefore represents an essential step toward the translational evaluation of human stem cells for long-term clinical applications.

SUPPLEMENTAL INFORMATION

Supplemental Information includes one figure, three tables, and Supplemental Experimental Procedures and can be found with this article online at doi:10.1016/j.stem.2012.04.021.

ACKNOWLEDGMENTS

This work was supported in part by a Grant-in-Aid from the Ministry of Agriculture, Forestry, and Fisheries of Japan. We thank staff in the Pig Management Section of the National Institute of Livestock and Grassland Science for assistance with animal management and Dr. T. Yagi for providing PKJ2 and MC1-DTA-p(A).

Received: November 17, 2011
Revised: March 13, 2012
Accepted: April 18, 2012
Published: June 13, 2012

REFERENCES

Asao, H., Okuyama, C., Kumaki, S., Ishii, N., Tsuchiya, S., Foster, D., and Sugamura, K. (2001). Cutting edge: the common gamma-chain is an indispensable subunit of the IL-21 receptor complex. J. Immunol. *167*, 1–5.

Cao, X., Shores, E.W., Hu-Li, J., Anver, M.R., Kelsall, B.L., Russell, S.M., Drago, J., Noguchi, M., Grinberg, A., Bloom, E.T., et al. (1995). Defective lymphoid development in mice lacking expression of the common cytokine receptor gamma chain. Immunity *2*, 223–238.

Felsburg, P.J., Hartnett, B.J., Henthorn, P.S., Moore, P.F., Krakowka, S., and Ochs, H.D. (1999). Canine X-linked severe combined immunodeficiency. Vet. Immunol. Immunopathol. *69*, 127–135.

Fischer, A., Cavazzana-Calvo, M., De Saint Basile, G., DeVillartay, J.P., Di Santo, J.P., Hivroz, C., Rieux-Laucat, F., and Le Deist, F. (1997). Naturally occurring primary deficiencies of the immune system. Annu. Rev. Immunol. *15*, 93–124.

Giri, J.G., Ahdieh, M., Eisenman, J., Shanebeck, K., Grabstein, K., Kumaki, S., Namen, A., Park, L.S., Cosman, D., and Anderson, D. (1994). Utilization of the beta and gamma chains of the IL-2 receptor by the novel cytokine IL-15. EMBO J. *13*, 2822–2830.

Ishii, N., Takeshita, T., Kimura, Y., Tada, K., Kondo, M., Nakamura, M., and Sugamura, K. (1994). Expression of the IL-2 receptor gamma chain on various populations in human peripheral blood. Int. Immunol. *6*, 1273–1277.

Ishikawa, F., Yasukawa, M., Lyons, B., Yoshida, S., Miyamoto, T., Yoshimoto, G., Watanabe, T., Akashi, K., Shultz, L.D., and Harada, M. (2005). Development of functional human blood and immune systems in NOD/SCID/IL2 receptor γ chain$^{(null)}$ mice. Blood *106*, 1565–1573.

Jiang, L., Lai, L., Samuel, M., Prather, R.S., Yang, X., and Tian, X.C. (2008). Expression of X-linked genes in deceased neonates and surviving cloned female piglets. Mol. Reprod. Dev. *75*, 265–273.

Kanai, N., Yanai, F., Hirose, S., Nibu, K., Izuhara, K., Tani, T., Kubota, T., and Mitsudome, A. (1999). A G to A transition at the last nucleotide of exon 6 of the gamma c gene (868G→A) may result in either a splice or missense mutation in

(I) Identification of immune subsets in recipient *Il2rg*$^{-/Y}$ male, #610, 12 weeks posttransfer as CD45RA$^+$CD3$^-$ B cells, CD3$^+$CD45RA$^+$ naive T cells, CD3$^+$CD45RA$^-$ memory T cells, and CD3$^-$CD16$^+$ NK cells among nonmyeloid and myeloid cells.
(J) Representative microsatellite PCR analyses to distinguish between donor and recipient DNA illustrated by the discriminatory marker (SW1263 for #610, SWR1367 for # 113, and SW24 for #122).
(K) Changes of IgG (left), IgA (middle), and IgM levels in serum from recipients (red lines) and wild-type controls (blue lines).

patients with X-linked severe combined immunodeficiency. Hum. Genet. *104*, 36–42.

Kimura, Y., Takeshita, T., Kondo, M., Ishii, N., Nakamura, M., Van Snick, J., and Sugamura, K. (1995). Sharing of the IL-2 receptor gamma chain with the functional IL-9 receptor complex. Int. Immunol. *7*, 115–120.

Kondo, M., Takeshita, T., Ishii, N., Nakamura, M., Watanabe, S., Arai, K., and Sugamura, K. (1993). Sharing of the interleukin-2 (IL-2) receptor gamma chain between receptors for IL-2 and IL-4. Science *262*, 1874–1877.

Leonard, W.J. (1996). The molecular basis of X-linked severe combined immunodeficiency: defective cytokine receptor signaling. Annu. Rev. Med. *47*, 229–239.

Nakamura, Y., Russell, S.M., Mess, S.A., Friedmann, M., Erdos, M., Francois, C., Jacques, Y., Adelstein, S., and Leonard, W.J. (1994). Heterodimerization of the IL-2 receptor beta- and gamma-chain cytoplasmic domains is required for signalling. Nature *369*, 330–333.

Nelson, B.H., Lord, J.D., and Greenberg, P.D. (1994). Cytoplasmic domains of the interleukin-2 receptor beta and gamma chains mediate the signal for T-cell proliferation. Nature *369*, 333–336.

Nelson, B.H., McIntosh, B.C., Rosencrans, L.L., and Greenberg, P.D. (1997). Requirement for an initial signal from the membrane-proximal region of the interleukin 2 receptor gamma(c) chain for Janus kinase activation leading to T cell proliferation. Proc. Natl. Acad. Sci. USA *94*, 1878–1883.

Noguchi, M., Nakamura, Y., Russell, S.M., Ziegler, S.F., Tsang, M., Cao, X., and Leonard, W.J. (1993a). Interleukin-2 receptor gamma chain: a functional component of the interleukin-7 receptor. Science *262*, 1877–1880.

Noguchi, M., Yi, H., Rosenblatt, H.M., Filipovich, A.H., Adelstein, S., Modi, W.S., McBride, O.W., and Leonard, W.J. (1993b). Interleukin-2 receptor gamma chain mutation results in X-linked severe combined immunodeficiency in humans. Cell *73*, 147–157.

Nolen, L.D., Gao, S., Han, Z., Mann, M.R., Gie Chung, Y., Otte, A.P., Bartolomei, M.S., and Latham, K.E. (2005). X chromosome reactivation and regulation in cloned embryos. Dev. Biol. *279*, 525–540.

Ohbo, K., Suda, T., Hashiyama, M., Mantani, A., Ikebe, M., Miyakawa, K., Moriyama, M., Nakamura, M., Katsuki, M., Takahashi, K., et al. (1996). Modulation of hematopoiesis in mice with a truncated mutant of the interleukin-2 receptor gamma chain. Blood *87*, 956–967.

Perryman, L.E. (2004). Molecular pathology of severe combined immunodeficiency in mice, horses, and dogs. Vet. Pathol. *41*, 95–100.

Puck, J.M., Nussbaum, R.L., and Conley, M.E. (1987). Carrier detection in X-linked severe combined immunodeficiency based on patterns of X chromosome inactivation. J. Clin. Invest. *79*, 1395–1400.

Russell, S.M., Keegan, A.D., Harada, N., Nakamura, Y., Noguchi, M., Leland, P., Friedmann, M.C., Miyajima, A., Puri, R.K., Paul, W.E., et al. (1993). Interleukin-2 receptor gamma chain: a functional component of the interleukin-4 receptor. Science *262*, 1880–1883.

Senda, S., Wakayama, T., Yamazaki, Y., Ohgane, J., Hattori, N., Tanaka, S., Yanagimachi, R., and Shiota, K. (2004). Skewed X-inactivation in cloned mice. Biochem. Biophys. Res. Commun. *321*, 38–44.

Shimozawa, N., Ono, Y., Kimoto, S., Hioki, K., Araki, Y., Shinkai, Y., Kono, T., and Ito, M. (2002). Abnormalities in cloned mice are not transmitted to the progeny. Genesis *34*, 203–207.

Shinkai, Y., Rathbun, G., Lam, K.P., Oltz, E.M., Stewart, V., Mendelsohn, M., Charron, J., Datta, M., Young, F., Stall, A.M., et al. (1992). RAG-2-deficient mice lack mature lymphocytes owing to inability to initiate V(D)J rearrangement. Cell *68*, 855–867.

Shultz, L.D., Lyons, B.L., Burzenski, L.M., Gott, B., Chen, X., Chaleff, S., Kotb, M., Gillies, S.D., King, M., Mangada, J., et al. (2005). Human lymphoid and myeloid cell development in NOD/LtSz-scid IL2R gamma null mice engrafted with mobilized human hemopoietic stem cells. J. Immunol. *174*, 6477–6489.

Takahashi, K., Tanabe, K., Ohnuki, M., Narita, M., Ichisaka, T., Tomoda, K., and Yamanaka, S. (2007). Induction of pluripotent stem cells from adult human fibroblasts by defined factors. Cell *131*, 861–872.

Takeshita, T., Asao, H., Ohtani, K., Ishii, N., Kumaki, S., Tanaka, N., Munakata, H., Nakamura, M., and Sugamura, K. (1992). Cloning of the gamma chain of the human IL-2 receptor. Science *257*, 379–382.

Traggiai, E., Chicha, L., Mazzucchelli, L., Bronz, L., Piffaretti, J.C., Lanzavecchia, A., and Manz, M.G. (2004). Development of a human adaptive immune system in cord blood cell-transplanted mice. Science *304*, 104–107.

Watanabe, S., Iwamoto, M., Suzuki, S., Fuchimoto, D., Honma, D., Nagai, T., Hashimoto, M., Yazaki, S., Sato, M., and Onishi, A. (2005). A novel method for the production of transgenic cloned pigs: electroporation-mediated gene transfer to non-cultured cells and subsequent selection with puromycin. Biol. Reprod. *72*, 309–315.

Journal of Thrombosis and Haemostasis, **10**: 1802–1813 DOI: 10.1111/j.1538-7836.2012.04851.x

ORIGINAL ARTICLE

Intra-articular injection of mesenchymal stem cells expressing coagulation factor ameliorates hemophilic arthropathy in factor VIII-deficient mice

Y. KASHIWAKURA,*† T. OHMORI,* J. MIMURO,* A. YASUMOTO,* A. ISHIWATA,* A. SAKATA,* S. MADOIWA,* M. INOUE,‡ M. HASEGAWA,‡ K. OZAWA§ and Y. SAKATA*

**Research Division of Cell and Molecular Medicine, Center for Molecular Medicine, Jichi Medical University; †Department of Immunology, Dokkyo Medical University School of Medicine, Tochigi; ‡DNAVEC Corporation, Ibaraki; and §Division of Genetic Therapeutics, Center for Molecular Medicine, Jichi Medical University, Tochigi, Japan*

To cite this article: Kashiwakura Y, Ohmori T, Mimuro J, Yasumoto A, Ishiwata A, Sakata A, Madoiwa S, Inoue M, Hasegawa M, Ozawa K, Sakata Y. Intra-articular injection of mesenchymal stem cells expressing coagulation factor ameliorates hemophilic arthropathy in factor VIII-deficient mice. *J Thromb Haemost* 2012; **10:** 1802–13.

Summary. *Background:* Transplantation of cells overexpressing a target protein represents a viable gene therapeutic approach for treating hemophilia. Here, we focused on the use of autologous mesenchymal stem cells (MSCs) expressing coagulation factor for the treatment of coagulation factor VIII (FVIII) deficiency in mice. *Methods and Results:* Analysis of luciferase gene constructs driven by different promoters revealed that the plasminogen activator inhibitor-1 (PAI-1) gene promoter coupled with the cytomegalovirus promoter enhancer region was one of the most effective promoters for producing the target protein. MSCs transduced with the simian immunodeficiency virus (SIV) vector containing the FVIII gene driven by the PAI-1 promoter expressed FVIII for several months, and this expression was maintained after multiple mesenchymal lineage differentiation. Although intravenous injection of cell supernatant derived from MSCs transduced with an SIV vector containing the FVIII gene driven by the PAI-1 promoter significantly increased plasma FVIII levels, subcutaneous implantation of the MSCs resulted in a transient and weak increase in plasma FVIII levels in FVIII-deficient mice. Interestingly, intra-articular injection of the transduced MSCs significantly ameliorated the hemarthrosis and hemophilic arthropathy induced by knee joint needle puncture in FVIII-deficient mice. The therapeutic effects of a single intra-articular injection of transduced MSCs to inhibit joint bleeding persisted for at least 8 weeks after administration. *Conclusions:* MSCs provide a promising autologous cell source for the production of coagulation factor. Intra-articular injection of MSCs expressing coagulation factor may offer an attractive treatment approach for hemophilic arthropathy.

Keywords: arthropathy, gene therapy, hemophilia, lentiviral vector, mesenchymal stem cells.

Correspondence: Tsukasa Ohmori or Yoichi Sakata, Research Division of Cell and Molecular Medicine, Center for Molecular Medicine, Jichi Medical University, 3111-1 Yakushiji, Shimotsuke, Tochigi 329-0498, Japan.
Tel.: +81 285 58 7397; fax: +81 285 44 7817.
E-mail: tohmori@jichi.ac.jp; yoisaka@jichi.ac.jp

Received 13 February 2012, accepted 28 June 2012

Introduction

Hemophilia is a recessive X-linked genetic bleeding disorder involving a lack of functional coagulation factor VIII (FVIII) or FIX. Hemophilia is considered to be suitable for gene therapy, because it is caused by a single gene abnormality, and therapeutic coagulation factor levels may vary across a broad range [1]. Although the objective of gene therapy is to correct a defective gene sequence responsible for a disease phenotype, recent studies have focused on ectopic expression of the target gene by viral or non-viral gene transfer [2,3]. Most gene therapy strategies for hemophilia are now exploiting two basic approaches: direct administration of a viral or plasmid vector for *in vivo* gene transfer, or transplantation of cells transduced *ex vivo* [2,3]. Adeno-associated virus (AAV) vectors have been extensively used for the former approach, and have shown dramatic efficacy in some animal models [4]. In fact, therapeutic levels of coagulation factor have also been achieved in patients with hemophilia B by use of the AAV8 serotype in a phase I clinical trial [5].

The other gene therapy strategy for hemophilia involves transplantation of cells transduced *ex vivo* to ectopically express coagulation factor [3]. We and others reported that transplantation of hematopoietic stem cells transduced with lentiviral vector expressing coagulation factor corrected the phenotype of mouse models of hemophilia [6–9]. In these studies, a blood cell lineage-specific promoter enabled the expression of coagulation factors in specific lineages of blood cells, including platelets [7,9], red blood cells [6], and

lymphocytes [10]. The use of blood cells to deliver coagulation factor is particularly attractive, as it avoids interference from circulating inhibitors [6,11]. Autologous hematopoietic stem cell-based gene therapy now represents an emerging therapeutic option for several immunodeficiency diseases [12]. However, the requirement for a conditioning regimen, including irradiation and/or chemotherapy, for successful transplantation means that this approach is not realistic for hemophilic patients.

Local implantation of cells expressing coagulation factor without conditioning treatments has been proposed as an alternative approach for cell-based therapy for hemophilia [13–15]. The advantage of locally implanting *ex vivo* transduced cells is that it avoids unexpected side effects caused by systemic influx of a viral vector. Many different types of cell have been reported to effectively express coagulation factor in cell-based therapy for hemophilia [13–16]. However, the emergence of a neutralizing antibody against coagulation factor or the loss of viability of the transplanted cells often limits their clinical applications, even if transient therapeutic expression of FVIII has been achieved [13,14]. Indeed, the transplantation of autologous fibroblasts expressing high levels of FVIII onto the omentum failed to achieve long-term expression of the coagulation factor in human clinical trials [16]. Clearly, further development of transplantation procedures is necessary before cell-based therapy can be successfully applied for hemophilic patients.

In this study, we focused on the use of mesenchymal stem cells (MSCs) as an autologous cell source to produce coagulation factor for cell-based gene therapy of a mouse model of hemophilia A. MSCs can be easily expanded *in vitro*, and effectively produce FVIII following lentiviral transduction. We found that the plasminogen activator inhibitor-1 (PAI-1) promoter was one of the most effective promoters for producing the target protein. Although we failed to consistently increase the plasma levels of coagulation factor after subcutaneous transplantation of the transduced cells in FVIII-deficient mice, we did confirm that the transduced MSCs elicited therapeutic effects by acting as a local hemostatic biomaterial in hemarthrosis and the resultant hemophilic arthropathy.

Materials and methods

The methods for construction of luciferase reporter plasmids, the luciferase reporter assay, the isolation of murine MSCs, the differentiation of MSCs, the subcutaneous transplantation of MSCs, histologic analysis and analysis of circulating FVIII inhibitors are described in detail in Data S1.

Mice

FVIII-deficient mice (B6;129S4-*F8*^{tm1Kaz}/J) [17] were kindly provided by H. H. Kazazian Jr (University of Pennsylvania, Philadelphia, PA, USA). C57BL/6J mice were purchased from Japan SLC (Shizuoka, Japan). All animal procedures were approved by the Institutional Animal Care and Concern Committee at Jichi Medical University, and animal care was in accordance with the committee's guidelines.

cDNA cloning, construction of lentiviral vectors, and virus production

The cDNAs for human B-domain-deleted FVIII (hBDD-FVIII) were generated as previously described [18]. The cDNAs for enhanced green fluorescent protein (EGFP), luciferase or hBDD-FVIII under the control of the indicated internal promoter were cloned into a self-inactivating simian immunodeficiency virus (SIV) lentiviral vector plasmid [19]. The SIV lentiviral vectors were generated essentially as previously described [7]. The transduction units of the lentiviral vector, transgene expression and proviral integration into the genomic DNA were measured as previously described [7,20].

Measurement of coagulation factor activity and antigen expression

Human hFVIII (hFVIII) antigen (hFVIII:Ag) was measured with an anti-hFVIII-specific ELISA kit (ASSERACHROM VIII:Ag; Diagnostica Stago, Seine, France). The functional activity of hFVIII (hFVIII:C) was measured with an activated partial thromboplastin time-based, one-stage clotting-time assay on an automated coagulation analyzer (Sysmex CA-500 analyzer; Sysmex, Kobe, Japan). We used pooled normal human plasma as a reference to measure both hFVIII:C and hFVIII:Ag.

Bioluminescence studies

The fates of transduced cells in identical recipient mice *in vivo* were directly assessed by measuring luciferase activities derived from the transduced cells (IVIS Imaging System and Living Image software; Xenogen, Alameda, CA, USA), as previously described [20].

Hemarthrosis model and intra-articular injection

The mouse model of hemophilic hemarthrosis was established by single needle puncture of the knee joints of FVIII-deficient mice, as previously described [21,22]. Briefly, 6–8-week-old mice were anesthetized with isoflurane, and the hair covering the left knee joint was shaved. The knee joint capsule was punctured with a 30-G needle below the patella to induce intra-articular bleeding. MSCs (1×10^5 cells per 5 μL) or vehicle alone (5 μL of saline) were directly injected into the affected knee joint with a Hamilton syringe (Hamilton, Bonaduz, Switzerland). The mice were allowed to recover. Then, at specified times after surgery, the mice were anesthetized with isoflurane, perfused with 50 mL of saline, and killed. Knee joints were collected by sectioning the femur and tibia, and macroscopic bleeding was photographed. Some knee sections were fixed and decalcified by the use of routine histologic procedures.